THEORETICAL AND COMPUTATIONAL MODELING OF AN IMPLANTABLE BIOMEDICAL DEVICE FOR LOCALIZED HYPERTHERMIA AND DRUG DELIVERY

A

Thesis Research

Presented to the Department of Theoretical Physics,

African University of Science and Technology, [Abuja]

in Partial Fulfillment of the Requirements for the Award of Master of Science (MSc)

in

Theoretical Physics

By

Bugase Jonas

Abuja, Nigeria

[October, 2011]

ACKNOWLEDGEMENT

My sincere gratitude goes to my creator for being my source of strength and life throughout this pursuit. The enormous knowledge and expertise of my supervisor Professor Wole Soboyejo has result in the success of this research and I remain very grateful to him.

Jing Du of Princeton University has also been very kind to me in taking time to teach me the fundamentals of the finite element simulation package Abaqus/CAE 6.9 in order to perform my simulation.

The unceasing support of my parents Mr. and Mrs. Bugase and my entire family has also contributed to the success of this work. I forever remain indebted to them all.

The special contribution of Ms. Juliet Sackey is duly appreciated. Those of Musty and Yahaya of the 2011 theoretical physics stream are also worth mentioning as well as all my colleagues in AUST. I am also grateful to all my friends back in Ghana for their continuous encouragement especially when times were very hard.

ABSTRACT

The advent of nanotechnology together with Biomedical Microelectro-Mechanical Systems (BioMEMS) for improved efficacy in treatment of cancer has resulted in the development of an implantable biomedical device for localized hyperthermia and drug delivery. This thesis work develops a mathematical framework based on relaxation losses of heating mechanism of magnetite magnetic nanoparticles synthesized with the Polydimethylsiloxane (PDMS) gel encasement. Numerical solution of the mathematical model developed showed explicit dependence of the temperature rise of the device on frequency and amplitude of the external applied field, relaxation time and volume fraction of the nanoparticles and implicitly on the viscosity of the PDMS gel and radius of the nanoparticles. A linear dependence of the temperature rise on the amplitude and frequency of the field was observed for usable range of values of the Radio Frequency field. Similarly for the viscosity of the gel and volume fraction the nanoparticles, it is approximately linear but saturates at a maximum value and then declines. This result was found to be in conformity with other predicted theoretical and experimental findings. This research shows that hyperthermia therapeutic temperature of 41 – 46^{o}C can achieved with frequency and amplitude ranges of 2.16 – 2.19 kHz and 9.77 – 9.89 kA/m respectively. Also, that for the range of the viscosity and volume fraction of the nanoparticles are 1.1 – 1.2 mPa.s and 0.12 – 0.14 respectively. Simulation of the heat diffusion profile of the implant and its surrounding tumor in 2D and 3D using a finite element simulation package Abaqus/CAE 6.9 showed that for maximum generated heat of 52^{o}C and 55^{o}C maintained the temperature of the tumor within the therapeutic range for more than thirty minutes. However, for a temperature 45^{o}C, the temperature falls a little below the therapeutic range but will be very useful in treatment for longer time periods. The generated heat in these cases is also seen to be enough to serve as the transition temperature for the thermosensitive drug loaded hydrogel embed in the device with micro channels for release since the drug release kinematic of the gel occurs between 37^{o}C and 45^{o}C.

TABLE OF CONTENTS

LIST OF FIGURES

LIST OF TABLES

CHAPTER ONE

BACKGROUND AND INTRODUCTION

1.1 BACKGROUND AND MOTIVATION

Cancer is identified as the seconding leading course of death by the World Health Organization (WHO). According to GLOBOCAN 2008 of the WHO, about 7.6 million cancer deaths occurred in 2008 and it is expected that there will be more than 13 million cancer deaths and approximately 21 million diagnosis by 2030 as reported by WHO in June 2010. Cancer diagnosis and treatment are of great interest due to the widespread occurrence of the disease, high death rate and reoccurrence after treatment [1]. The disease is widespread regardless of race, and occurs in many sites including lung, breast, kidney, ovary, prostate, colon, bladder, and cervix. With increasing industrialization and other socio-behavioral changes in most developing countries, and Sub-Saharan Africa as a whole, it is projected by the WHO that the rate of incidence of cancer will increase to the leading cause of death by 2030.

There are several conventional approaches to cancer treatment; these include surgery, radiation, hormone, gene, immunotherapy, etc. with radiation, surgery and chemotherapy being the most common [2]. Most widely acknowledged issues with chemotherapy are the exposure of healthy tissues to toxic chemicals and the inefficiency of achieving the therapeutic zone [3]. Among other conventional treatment are hormone therapy, radiation therapy, surgery and thermal therapy. However, an integrated approach to cancer treatment that is promising, and currently at the heart of research, is the combination of radiotherapy, chemotherapy, surgery and hyperthermia.

Electronic devices have now reached a stage of dimensions comparable to those of biological macromolecules. This raises exciting possibilities for combining microelectronic and biotechnology to develop new technologies with unprecedented power and versatility [4]. The plethora of biomedical microelectromechanical systems (BioMEMS) emerging today range from fascinating molecular motors that swim inside a cell utilizing the intercellular energy-rich ATP molecules to sophisticated point-of-care diagnostic devices [5].

Magnetic nanoparticles (MNPs) mainly magnetic elements of iron, cobalt, nickel and their chemical compounds in recent times have numerous applications in data storage, Magnetic Resonance Imaging (MRI), and Biomedicines especially as agents for heating, temperature sensoring and drug delivery in biomedical devices. In general, Nano sized magnetic particles display superparamagnetism with properties dependent on the synthesis and chemical structure. Shell materials for magnetic nanoparticles used for medical applications include polysaccharides for example dextron or derivatives (carboxymethylated dextran, Poly(ethyleneglycol), Poly(N-isoproply-acrylamide) e.t.c [6]. However, the most commonly used are ferrite nanoparticles which exhibit agglomeration and according to K. Babinch et al [6], iron oxides have known low cytotoxicity and high biocompatibility.

In particular, magnetic nanoparticles can be localized in deep tissue, external static magnetic field can fix them at precise position, gradient fields can move them and alternating (AC) fields lead to local heating. The latter can be utilized for hyperthermia applications which are shown for example by the use of superparamagnetic nanoparticles for magnetic fluid hyperthermia [7].

A great advantage of magnetic field is their biocompatibility, i.e. they penetrate tissue non-invasively and without known adverse effects and their weak interaction with organic matter so that deep layers of human tissue can be reached [7]. To this end, a magnetic field is applied to the biomedical device and heat induced by the magnetic nanoparticles for localized hyperthermia.

The challenge of targeted drug delivery, coupled with the advent of nanotechnology, has led to the discovery and development of novel biomedical devices for localized hyperthermia and drug delivery. These devices will reduce the effects of bulk systemic treatments and increase the effectiveness of localized treatments by controlling drug release. These devices are currently under intense research by material scientists, engineers and medical practitioners.

In this novel device, thermosensitive drug loaded hydrogel (PNIPA) is encapsulated in a biocompatible gel (Polydimethylsiloxane microfluidic devices, PDMS) [3]. Several thermosensitive polymer hydrogels have proven to be biocompatible. These hydrogels are advantageous in clinical application due to their fluidity below lower critical solution

temperature at approximately 33 ^{o}C which enable them to be introduced into site-specific organ, tissue or body cavity with improved applicability and comfort of injection [8].

The PDMS gel is synthesized with magnetic nanoparticles which induce heat by hysteresis, when an external alternating (AC) magnetic field is applied. The heat is used for localized hyperthermia for cancer treatment, and also in drug delivery, since the hydrogel is temperature sensitive and shrinks to expel drug, when the temperature of the device is increased. Essentially, this process controls the amount of drug released and to specific or targeted location.

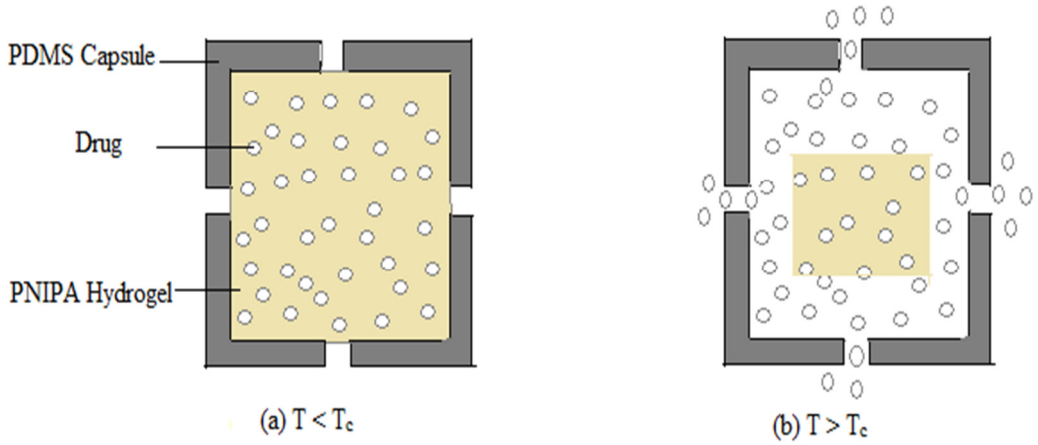

Fig 1.0: Schematic diagram of Hydrogel, PNIPA encapsulated by a biocompatible gel PDMS

1.2 SCOPE OF WORK

This thesis presents a theoretical/computational framework of the modeling of the heating a localized nanocomposite gel for the treatment of cancer by hyperthermia. The effects of applied magnetic field are modeled using a combination of electromagnetic theory and thermodynamics concepts. The heat diffusion is also modeled within a computational framework that explores the potential for future application in the localized treatment of breast cancer via hyperthermia.

The thesis is divided into five chapters. Following the introduction, the literature review is presented in chapter two. The theoretical and computational models are then described in chapter three before comparing the predictions to experimental work by Oyku Akkaya. Conclusions will be drawn in chapter four while future work presented in chapter five.

CHAPTER TWO

LITERATURE REVIEW

2.1 INTRODUCTION

The impact of high incidence of cancer and death rates in both developed and developing countries has resulted in the increased need for effective diagnose and treatment of the disease. To this end, the combined effect of chemotherapy, radiation therapy and other therapeutic approaches is explored. The use of magnetic nanoparticles for improved drug delivery systems and hyperthermia is extensively studied for cancer treatment. This chapter presents an overview of prior work and survey of relevant literature.

2.2 CANCER AND CANCER TREATMENT

According to the World Cancer Report from the International Agency for Research on Cancer in December 2008, there is an expected global annual increase of one percent (1%) in cancer incidence making it leading cause of death by 2030. The reasons for the increased rates are due to the increased rate of adoption of tobacco use and high-fat diet in less developed countries and demographic changes including a projected population increase of thirty-eight percent in less developed countries between 2008 and 2030.

In general, cancer is a deadly known disease that is characterized by uncontrolled growth and spread of abnormal cells that form tumors. All cancers involve the malfunction of genes that control cell growth and division [2]. These tumors usually alter the nervous, digestion and circulatory system because they secret unwanted hormones. Cancer is caused by both external and internal factors. External factors include tobacco, infectious organisms, chemicals and radiation while the internal factors are inherited mutation, hormones and immune conditions [2].

The time of detection of the disease strongly influences the success of treatment. Cancers can be diagnosed at different states in their development. The stage of cancer diagnose may be expressed as ‘Localized’, ‘Regional’, and ‘Distant’ or by numerals I, II, III, or IV where the more localized or lower the number, the likely treatment will be effective [9]. The three main types of treatment for cancer are surgical therapy, radiation therapy and chemotherapy. Others

therapeutic approaches include gene therapy, hormone therapy and immunotherapy [10]. Depending on the stage and type of cancer, treatment might involve the combination of any of the conventional approaches.

Surgery is a clinical method of removing the tumor from the body of the patient and most effective when the disease has not spread to other parts. Chemotherapy involves the use of chemical and antineoplastic drugs by intravenously administering these drugs destroying the cancer cell in the entire body. Bulk systemic administering however results in undesired destruction of healthy cells since large amounts of drug is administered with only one percent (1%) reaching the targeted cell consequently affecting the immune system of patients [11]. There is therefore the need for controlled drug delivery in chemotherapy. Targeted drug delivery systems including chemotherapy wafers, microchips, polymer-drug conjugate among others are currently being developed and used.

Fig 2.0: Microchips and wafers used for localized drug delivery [3]

Radiation therapy is the process of using high energy electromagnetic waves e.g. X-rays for attacking and damaging cancer cells. The high-dose modifies the genetic makeup of the cells preventing reproduction. The exposure of healthy tissues to radiation also has unavoidable consequences.

2.3 HYPERTHERMIA IN CANCER TREATMENT

Hyperthermia is the abnormal increase of the body's temperature. This temperature increase has been identified by oncologist as a therapeutic effect for cancer treatment in recent times. Hyperthermia also refers to the body temperature elevated for therapeutic reasons. It has been observed that cancer cells are more temperature sensitive than normal cells in the therapeutic

temperature range of 42-45^{o} C and improves the efficacy of other treatments like chemotherapy and radiotherapy [12]. The different response is based on physiological properties of the normal and cancerous cell.

Increased temperature for cancer treatment can be classified as hyperthermia or thermoablation. Hyperthermia causes cell death known as apoptosis at temperature range of 41-45^{o}C. Apoptosis is a genetically programmed and biochemically active mode of death in which the cell actively participates in its own elimination and do not elicit an inflammatory response [13]. On the other hand, thermoablation occurs at high temperature of 50^{o}C and above resulting in tissue necrosis. In necrosis cell death, there is a decline in ATP production, mitochondrial swelling and eventually cytolysis and the release of pro-inflammatory agents which is toxic cell material [13].

Hyperthermia in cancer treatment can be local, regional, or entire body which may involve the application of heat to the treat tumors by focusing microwaves, lasers, ultrasound and magnetic energy or use of thermal chambers. Hyperthermia cancer treatment is bedeviled with the damage of healthy tissue in the process and difficulty of treating deep-seated tumors. After considerable research however, magnetically mediated hyperthermia has be found to live up to these challenges and poses a non-invasive procedure [12].

Among other magnetically mediated hyperthermia methods, Magnetic Fluid Hyperthermia has been recently identified as a promising biomedical tool for cancer treatment.

2.3.1 MAGNETIC FLUID HYPERTHERMIA (MFH)

Magnetic Fluid Hyperthermia (MFH) uses small size magnetic nanoparticles that are superparamagnetic in contrast to large ferromagnetic thermoseeds used in other forms of magnetically mediated hyperthermia. The small size nanoparticles can be non-invasively introduced into tissues and also results in uniform temperature distribution due to their well disperse nature within the tissue [12]. Magnetic fluid hyperthermia in cancer treatment involves the injection of fluid containing magnetic nanoparticles in tumors such that an applied radiofrequency (RF) alternating magnetic field consequently result in tumor destruction stemming from nanoparticle heat generation [14].

According to Tartaj et al [15], a magnetic fluid consists of dispersed magnetic nanoparticles in water at a neutral PH and physiological salinity. The colloidal stability of the fluid is dependent on the particle dimension and surface chemistry where small sized particles are preferred due to their effective surface area, low sedimentation rate or high stability and improved tissular diffusion. The biocompatibility of the nanoparticles is also of great concern hence; they are usually coated with biocompatible polymers before or after synthesis process. Magnetite (Fe_3O_4) is preferred as a heating agent for effective magnetic fluid hyperthermia in cancer treatment due to its known strong magnetic properties and low toxicity [16].

The uniform nanoparticle size and shape, the size distribution, surface chemistry and consequently the magnetic properties is determined to a large extend by the synthesis process of these nanoparticles [15]. For biomedical application, the synthesis methods include solution chemistry and aerosol/vapour technique.

Homogeneous precipitation involves the formation and growth of particles. Nucleation occurs when the constituent concentration reaches critical supersaturation. Following the nucleation process is the uniform growth of the nuclei by diffusion of solute from the solution to their surface until the final size is attained [15]. The formation of particles during the growth stage should be avoided and separation of the two stages for monodispersity.

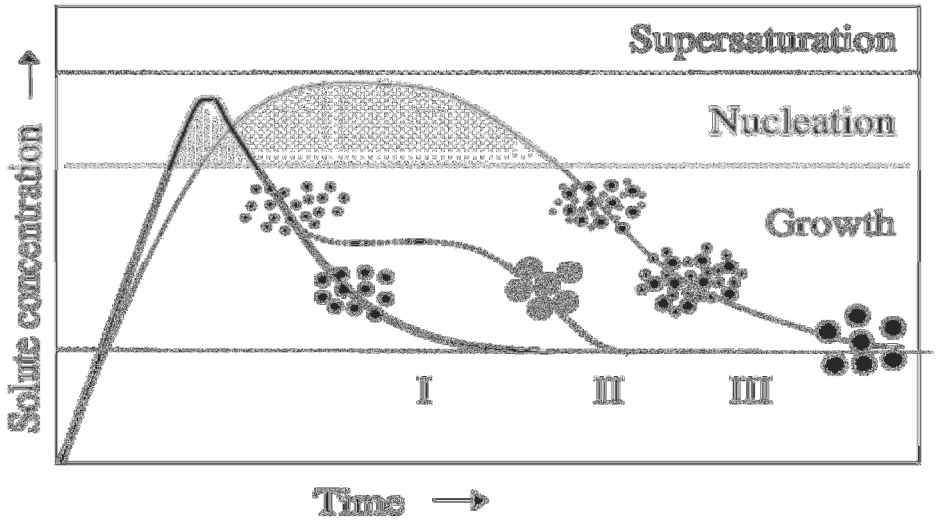

Fig 2.1: Mechanism of formation of uniform particles in solution: (I) single nucleation and uniform growth by diffusion (classical model of LaMer and Dinegar); (II) nucleation, growth and aggregation of smaller subunits; (III) multiple nucleation events and Ostwald ripening growth [15]

Spray and laser pyrolysis are techniques of Aerosol/Vapor method of synthesizing well-defined magnetic nanoparticles for both *in vivo* and *in vitro* applications [15]. In spray pyrolysis, a solid is obtained by spraying a solution into series of reactors where evaporation of solvent and condensation of solute within the aerosol droplets occur. Drying and thermolysis is done at high temperatures. Laser pyrolysis employs continuous wave carbon dioxide laser for initiating the nanoparticle formation reaction and result in narrow particle size distribution with little or no particle aggregation [14].

The synthesized magnetic fluid is localized in tumors for magnetic fluid hyperthermia treatment by various methods based on the nature and location of the tumors. According to J. L. Phillips review of magnetic fluid hyperthermia MFH, direct injection concentrates fluid in tumors whose location has been identified. The fluid may also be injected intravenously and the particles transported to regions of interest by blood circulation [17]. Small tumors without specified locations can also be treated by this method of administering the nanoparticles and applying the field only to tumor regions. A more improve method involves attaching targeting antibodies to nanoparticles which will concentrate them in cancerous cells for treatment.

The tissue temperature in MFH is strongly dependent on the magnetic properties of the material used, frequency and strength of the applied field, blood perfusion in the tissue and the duration of application of the field.

2.3.2 LOW CURIE TEMPERATURE NANOPARTICLES

In magnetic fluid hyperthermia MFH, the heat generated by the magnetic nanoparticles must maintain the temperature of the tumor above the therapeutic threshold of $42^{o}C$ for thirty minutes (30min) or more in order to destroy the tumor [18]. The unfortunate possible local overheating and necrosis of normal tissue during hyperthermia is of great concern. Therefore, careful selection of parameters and means of monitoring the heat generated and temperature is desired.

Choosing magnetic materials with Curie temperature equal to the therapeutic temperature will solve this problem [12]. Curie temperature is defined as the temperature at which the magnetic material (ferromagnetic or ferrimagnetic) losses its magnetic momentum becoming paramagnetic and heating function is based on Néel Relaxation which can be altered through material composition and nanoparticle size [19]. Magnetic materials with Low-Curie temperature will produce heat until they reach the Curie temperature where they become ineffective unless they their temperature falls below the Curie temperature.

A magnetic material with Curie temperature equal to the therapeutic temperature will act as self-controller generating heat only when below the therapeutic temperature. Self-regulating nanoparticles ensures that the tumor reaches the desired temperature for treatment without affecting normal tissue, hence being referred to as Self-Regulated Magnetic Fluid Hyperthermia.

2.4 BIOMEMS FOR HYPERTHERMIA

The science of biomaterials and their applications are tremendous in recent years. Biomaterials are defined as nonviable materials used in medical devices intending to interact with biological systems and their biocompatibility being their ability to perform with an appropriate host response in a specific application [20].

The advent of micromachining, Microelectro-Mechanical Systems (MEMS) and microsystem technology has opened a new gate for design and fabrication of miniature biomedical devices for a verity of applications such as drug delivery systems, Lab-on-a-chip among others [21]. The application of microelectro-mechanical systems (MEMS) in biological and biomedical systems cannot be over emphasized. Bio-Micro-Electro-Mechanical Systems (BioMEMS) are small length scale devices that have diagnostic and therapeutic applications including biosensors, chemical analysis systems, cell encapsulation, DNA sequencing and drug delivery [22].

In general, silicon and glass are the main materials used in micromachining and MEMS but most biomedical devices uses soft or polymeric or gel materials such as silicone rubber, polycarbonate, lsobonyl acrylate and polyimide. The basic fabrication methods in micromachining and MEMS are thin film deposition, lithography, etching and substrate bonding [21].

BioMEMS are fabricated by soft lithography in the process of molding and embossing of silicone rubber otherwise known as polydimethylsiloxane (PDMS). The biocompatibility of this polymer together with other properties makes it suitable for microfluidic. As a result, most BioMEMS are used in drug delivery systems through biocapsules, microneedles, micropumps and microreservoir devices. The use of these devices has been seen to improve drug delivery and subsequently the therapeutic efficacy of drugs.

Current research has also focused on the use of BioMEMS for hyperthermia in treatment of cancer. BioMEMS are fabricated into implantable devices where they are intended to increase the temperature of the surrounding tissue to a therapeutic value. This temperature rise is achieved through either resistive heating or inductive heating of the device.

In the case if resistive heating, an electrical circuit is incorporated in the device that allows the supply of current to generate heat. This involves attaching a coil of wire to the implant and sometimes referred to as joule heating. With regard inductive heating, magnetic nanoparticles are added to the PDMS gel during the fabrication of the device. An external applied magnetic field will then induce heat in the device due to electromagnetic mechanisms of hysteresis losses, relaxation losses, eddy currents, or resonance losses.

The use of BioMEMS for both localized hyperthermia and drug delivery has also shown interesting potential where the heat generated for hyperthermia can also assist in controlled drug delivery by loading the device with temperature sensitive drug load-loaded hydrogels.

2.5 ELECTROMAGNETIC RADIATION AND ELECTROMAGNETISM

Electromagnetism and electromagnetic radiations form one of the four fundamental interactions in nature. These phenomena describe energy and energy interaction that is seen in the interrelated magnetic and electric fields. Electrodynamics being the physics of electromagnetic radiation is predicted by the classical laws of electricity and magnetism in Maxwell's equations without source. The basic concepts of these phenomena are considered in this section.

2.5.1 ELECTROMAGNETIC RADIATION

Electromagnetic Radiations (EMR) are energy carrying waves that have both magnetic and electric field components which oscillate in phase perpendicular to each other and to the direction of propagation. The radiations are classified in order of increasing frequency and decreasing wavelength in a spectrum known as the electromagnetic spectrum. In this spectrum, radiations with high frequencies have high energy since shorter wavelengths results in higher energies. In order of increasing energy, EM waves are categorized as radio waves, microwaves, infrared radiations, visible light, Ultraviolet (UV) rays, X-rays, and Gamma rays.

The interaction between EM radiations and matter is dependent on the energy of the radiation or the part of the EM spectrum involved. According to American Cancer Society, radiations are categorized into ionizing and non-ionizing where ionizing radiations have enough energy to liberate an electron from an atom or molecule whereas non-ionizing radiations do not. High frequency radiations such as X-rays, gamma rays and some high UV rays are considered ionizing radiations and carcinogens since they cause damage to DNA, RNA, proteins among others. Non-ionizing radiations do not directly damage biological molecules and include radio waves, microwaves, infrared rays, visible light and low UV rays. Besides UV rays, these radiation typically show no risk of cancer.

Biomedical application of EM radiations is seen in a wide range of cancer diagnostic and therapeutic techniques which involve both direct and indirect emission and detection of EM waves such as X-ray radiography, Computer Tomography Scanning (CT Scan), gamma-ray radiography, Positron Emission Tomography (PET), Magnetic Resonance Imaging (MRI), and Microwave Hyperthermia (MWH) [23]. Below is a schematic showing different ranges of EM spectrum, different techniques, physical and biological phenomena that occur in these ranges.

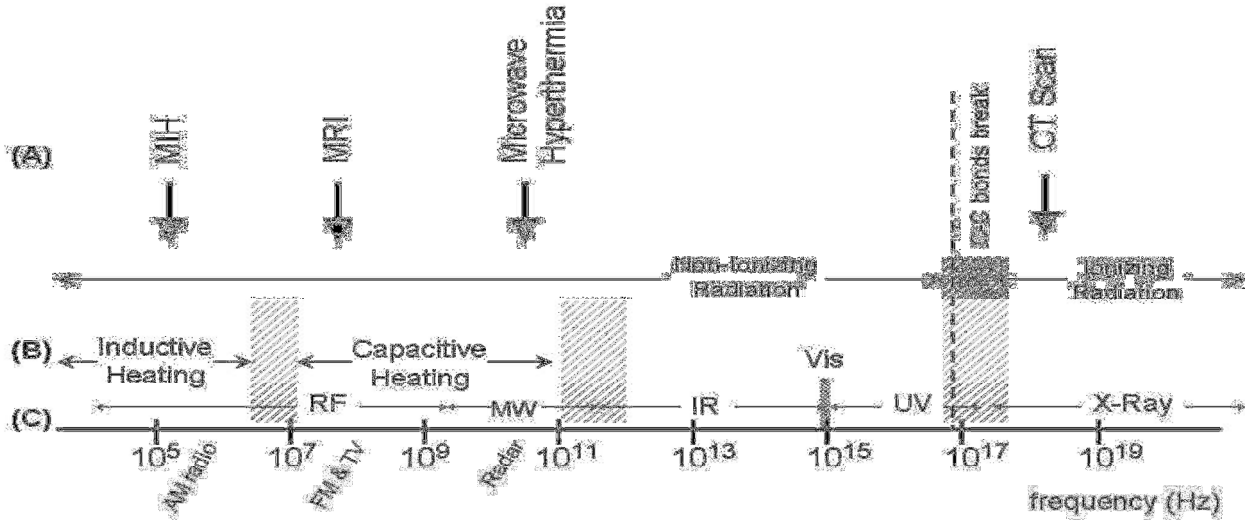

Fig 2.2: (A) Frequency ranges for some of the most used diagnostic/therapy techniques (MFH = Magnetic Fluid Hyperthermia), (B) The main physical mechanisms at each frequency range, (C) common nomenclature for the EM waves at each region: RF = radiofrequency, MW= microwaves, IR = infrared, Vis = visible, UV = ultraviolet and X-rays [23]

According to Goys et al [23], organic materials composed of long-chained carbon molecules can absorb EM radiations at specific frequencies e.g. covalent bonds are broken at approximately 10^{12}Hz ($\lambda \approx 300$nm in UV range). This tends to be biologically dangerous.

The physics of EM radiation is known as electrodynamics and is predicted by the classical laws of electricity and magnetism in Maxwell's equations.

2.5.2 BASIC LAWS OF ELECTROMAGNETISM

In the nucleus of atoms, a nonelectrical force called Nuclear force holds the protons together which is much greater than the electrical repulsion [24]. The electrical forces exist between electrons and similarly, the nuclear force obeys the inverse-square law. This force is sometimes known as the columbic force the law referred to as Coulomb's law of electrostatics.

Gravitational force, electrical force, among others obey the inverse-square law which states that the force on a charge (q) due to a point charge (Q) is proportional to the product of the two charges and inversely proportional to the square of the distance (r) between them [25]. This law is given mathematically as;

$$F = \frac{qQ}{4\pi\varepsilon_0 r^2} \tag{2.0}$$

where ε_o is the permittivity of free space and given to be 8.85 X 10^{-12} $C^2N^{-1}m^{-2}$

For many materials, including metals, experiments show that the resistance remains constant over wide range of applied voltages or currents. Ohm's law states that the current (I) flowing through a wire or electrical conductor is proportional to the potential drop (V) along the wire. Materials that obey Ohm's law are termed ohmic in nature. The constant of proportionality is known as the resistance (R) and measured in ohms (Ω).

$$V = IR \tag{2.1}$$

In general, the Ohm's law is given in terms of the electric field (E), current density (j) and the resistivity (ρ) or conductivity (σ) of the material.

$$E = \rho j \tag{2.2}$$

$$\sigma = \frac{1}{\rho} \tag{2.3}$$

The current density (j) is a vector, parallel to the flow of charge, whose magnitude is the amount of charge per unit time crossing a unit area perpendicular to the flow.

$$j = -neV \tag{2.4}$$

Where n is the electron density, e is the charge of the electrons and V is the velocity of the electrons.

In electromagnetism, the force that acts on a charge is dependent on the position of the charge, its velocity and the amount of other charges that act on it. The magnetic force on a charge (Q) moving with velocity v in a magnetic field (B) is known as Lorentz force [25].

$$F_{mag} = Q(v \times B) \tag{2.5}$$

In the presence of both a Magnetic field (B) and Electric field (E) which are both vector fields, the, the Lorentz force is given as;

$$F = q(E + v \times B) \tag{2.6}$$

The total Lorentz force combined with the equation of motion of a particle is given as;

$$\frac{d}{dt}\left[\frac{mv}{\left(1-\frac{v^2}{c^2}\right)^{\frac{1}{2}}}\right] = q(E + v \times B) \tag{2.7}$$

The unit of magnetic field (B) is $NsC^{-1}m^{-1}$ or Vsm^{-2} or Weber per square meter.

2.5.3 MAGNETISATION AND MAGNETISING FIELD

In the analysis of the properties of stationary magnetic media and associated currents, the true current j^{true}, Polarization currents $\frac{\partial P}{\partial t}$ and the magnetization currents j^m were identified [26]. In Dirac's symmetrized form of electrodynamics, the Maxwell's equations are written as;

$$\nabla \cdot E = \frac{\rho\, e}{\varepsilon_o} \tag{2.8}$$

$$\nabla \times E = -\mu_0 j^e - \frac{\partial B}{\partial t} \tag{2.9}$$

$$\nabla \cdot B = \mu_0\, \rho^m \tag{2.10}$$

$$\nabla \times B = \mu_0 j^e + \varepsilon_o \mu_0 \frac{\partial B}{\partial t} \tag{2.11}$$

The influence of external electric field on free charges and the effects on a bulk material result in the electric polarization P and magnetizing field H. The electric displacement vector D is related to the electric field and polarization by the equation;

$$\mathrm{D} = \varepsilon_o \mathrm{E} + \mathrm{P} \tag{2.12}$$

Taking the divergence of equation (2.12),

$$\nabla \cdot \mathrm{D} = \nabla \cdot (\varepsilon_o \mathrm{E} + \mathrm{P}) \tag{2.13}$$

But $$\nabla \cdot \mathrm{D} = \rho^{\mathrm{true}}(\mathrm{x}) \tag{2.14}$$

$$\rho^{\mathrm{pol}} = -\nabla \cdot \mathrm{p} \tag{2.15}$$

$$\rho^{\mathrm{total}} = \rho^{\mathrm{true}} + \rho^{\mathrm{pol}} \tag{2.16}$$

Where ρ^{total}, ρ^{true}, and ρ^{pol} are the 'total' charge, 'true' charge and 'polarized' charge densities respectively. Hence, Maxwell's equation (2.8) becomes;

$$\nabla \cdot \mathrm{E} = \frac{\rho^{\mathrm{total}}{}_{(x)}}{\varepsilon_o} \tag{2.17}$$

The electric field strength and polarization are related by the electric susceptibility (χ) by the equation;

$$\mathrm{P} = \varepsilon_o \chi \mathrm{E} \tag{2.18}$$

Therefore, the electric displacement vector D can be rewritten as;

$$\mathrm{D} = \varepsilon_o \mathrm{E} + \varepsilon_o \chi \mathrm{E} \tag{2.19}$$

$$\mathrm{D} = \varepsilon \mathrm{E} \tag{2.20}$$

where $\varepsilon = \varepsilon_o(1 + \chi)$ is the permittivity of the material

The magnetic dipole moment (m) which is analogous to the electric dipole moment is defined as

$$\mathrm{m} = \frac{1}{2}\int_{V'} \mathrm{d}^3x' \, (x' - x) \times \mathrm{j}(x') \tag{2.21}$$

Magnetization (M) is the magnetic dipole moment per unit volume of a material [26]. This is defined in terms of the magnetization current j^m.

$$j^m = \nabla \times M \tag{2.22}$$

The magnetizing field H is defined in terms of the magnetic field strength B and magnetization of the material as;

$$H = \frac{B}{\mu_0} - M \tag{2.23}$$

$$M = B - \mu_0 H \tag{2.24}$$

Also, the magnetizing field H is defined in terms of the magnetic susceptibility χ_m as;

$$H = \frac{B}{\mu_0 (1+\chi_m)} \tag{2.25}$$

$$H = \frac{B}{\mu} \tag{2.26}$$

The permeability of the material is $\mu = \mu_o(1+\chi_m)$.

In the quantum mechanical regime, the magnetization M of a quantum mechanical system of volume V in a uniform magnetic field H is defined as [27];

$$M(H) = -\frac{1}{V}\frac{\partial E_o(H)}{\partial H} \tag{2.27}$$

E_o is the ground-state energy in the presence of the magnetizing field.

With regards thermodynamics, the magnetization is the partial derivative of the magnetic Helmholtz free energy (F) with respect to the magnetic field H [27].

$$M(H) = -\frac{1}{V}\frac{\partial F}{\partial H} \tag{2.28}$$

$$\chi_m = \frac{\partial M}{\partial H} = -\frac{1}{V}\frac{\partial E_o(H)}{\partial H} \tag{2.29}$$

2.5.4 MAGNETIC INDUCTION

The force on a current carrying conductor in the presence of a magnetic field is given as;

$$F = \oint_L Idl \times B \tag{2.30}$$

Where B is the force per unit current element or magnetic flux density

Bio-Savert law states that a current carrying conductor of elemental length *dl* in the direction of the current and coordinate vector x from an observation point has an elemental magnetic flux density *dB* given as;

$$dB = \mathrm{KI}\ \frac{dl \times x}{|x|^3} \tag{2.31}$$

The flux density of the charge in motion is therefore

$$B = Kq\ \frac{V \times x}{|x|^3} \tag{2.32}$$

K = 1/C C is the speed of light. $K = \mu_o/4\pi = 10^{-7}\ N/A^2$

The magnetic induction in terms of the current density J(x)

$$B(x) = \frac{\mu_o}{4\pi} \int J(x) \times \frac{x - x'}{|x|^3}\ d^3x' \tag{2.33}$$

The magnetic induction field lines for a current carrying wire are concentric circles around the wire and the magnitude of the magnetic induction B from a distance R to an observer is given by [28];

$$|B| = \frac{\mu_o IR}{4\pi} \int_{-\infty}^{\infty} \frac{dl}{(R^2 + l^2)} = \frac{\mu_o I}{2\pi R} \tag{2.34}$$

In a closed loop, the magnetic dipole moment measured in A/m^2 is the product of the current and the area of the loop with its direction normal to the loop.

$$\mathrm{m} = \mathrm{ISa_n} \tag{2.35}$$

where S is the loop area and a_n is the unit normal vector to the plane of the loop.

For a stationary closed loop with current flowing through it, the magnitude of the magnetic field is proportional to the current.

$$B(x) = \frac{\mu_o}{4\pi} \int_\Gamma \frac{dl\,(x-x')}{|x-x'|^3} \tag{2.36}$$

Hence, the magnetic flux Φ is also directly proportional to the current with the constant of proportionality being the Mutual Inductance due to another current carrying loop [29].

$$\Phi = MI \tag{2.37}$$

The mutual inductance of tow loops is dependent on the geometry of the loop i.e. shape, size and orientation. Hence,

$$\Phi = \mathcal{L}I \tag{2.38}$$

$\mathcal{L}$ is the self-inductance

The Faraday's law of electromagnetic induction gives a relation between the electric field and the changing magnetic field as;

$$\nabla \times E = -\frac{\partial B}{\partial t} \tag{2.39}$$

From Stoke's theorem,

$$\oint_\Gamma E.ds = \oint_S (\nabla \times E) \cdot \hat{n} da = -\oint_S \frac{\partial}{\partial t} B \cdot \hat{n} da \tag{2.40}$$

$$\oint_\Gamma E.ds = -\frac{d}{dt} \oint_S B \cdot \hat{n} da = -\frac{d}{dt}\Phi = \mathcal{E} \tag{2.41}$$

Therefore, flux $\Phi = \oint_S B \cdot \hat{n} da$ and $\mathcal{E}$ being electromotive force, $\hat{n}$ is unit normal vector, S the surface bounded by the closed curve Γ and a being the surface area [24].

The self-induced electromotive force ($\mathcal{E}$) in a coil is proportional ot the rate of change of current flowing through it.

$$\mathcal{E} = -\mathcal{L}\frac{dI}{dt} \tag{2.42}$$

2.5.5 INDUCTANCE AND MAGNETIC ENERGY

Momentum in a coil due to an induced electromotive force is the product of the self-inductance and the current in it. The rate of electrical work is given as;

$$\frac{dw}{dt} = \mathcal{E}I = -\mathcal{L}\frac{dI^2}{dt} \tag{2.43}$$

Magnetic energy $U = \frac{1}{2}\mathcal{L}I^2$

Magnetic energy for a distribution of stationary current is also given as

$$U = \frac{1}{2}\int J \cdot AdV \tag{2.44}$$

$$\mathcal{L} = \frac{1}{I^2}\int J \cdot AdV \tag{2.45}$$

J and A are the current density and vector potential of the field.

Magnetic energy in terms of the magnetic field B is given as a function of the current density and vector potential;

$$U = \frac{\varepsilon_o C^2}{2}\int (\nabla \times B) \cdot AdV \tag{2.46}$$

2.6 MAGNETIC MATERIALS

Magnetic materials are primarily Iron, Nickel, Cobalt and their alloys. Magnetic materials have a microscopic origin being magnetic moments of the atoms that composes the material. In an atom, the magnetic moment has contribution from both the orbital and spin motion of electrons.

$$\vec{m} = -2\mu_B \vec{S} - \mu_B l \tag{2.47}$$

$\mu_B = \frac{e\hbar}{2mc}$ is the Bohr magneton.

The magnetic property of a solid material is also affected by the electronic configuration of the constituent atoms. The net magnetic moment of an atom is different from zero if the shells are not completely filled. The magnetic induction B and magnetic field H are related by the magnetic permeability of the material μ.

$$B = \mu H = \mu_o \mu_r H \tag{2.48}$$

$$\mu_r = 1 + \chi \tag{2.49}$$

$$\vec{M} = \chi \vec{H} \tag{2.50}$$

μ_r and μ_o are the relative permeability and permeability of free space respectively. χ is the magnetic susceptibility of the material. The magnetic susceptibility and relative permeability of a material depend on the chemical composition, structure, temperature, magnitude of the applied field and the history of exposure of the material to a field. Magnetic materials are classified into three (3) major materials; Diamagnetic, Paramagnetic and Ferromagnetic. Others include Ferrimagnetic and Antiferromagnetic materials.

Diamagnetic materials have a no net magnetic moment in the absence of an applied field possesses a net magnetic moment that tends to oppose the applied field. They have a small and negative magnetic susceptibility in the order of 10^{-5} which is temperature independent and a relative permeability $\mu_r \leq 1$. The effect of diamagnetism in is microscopic and not easily observed for bulk materials. Examples of such materials include Bismuth, Mercury, Lead, and Sliver. Solids that are composed of ions with filled electron shells have zero spin and angular moments and therefore a Larmor Diamagnetic Susceptibility [26].

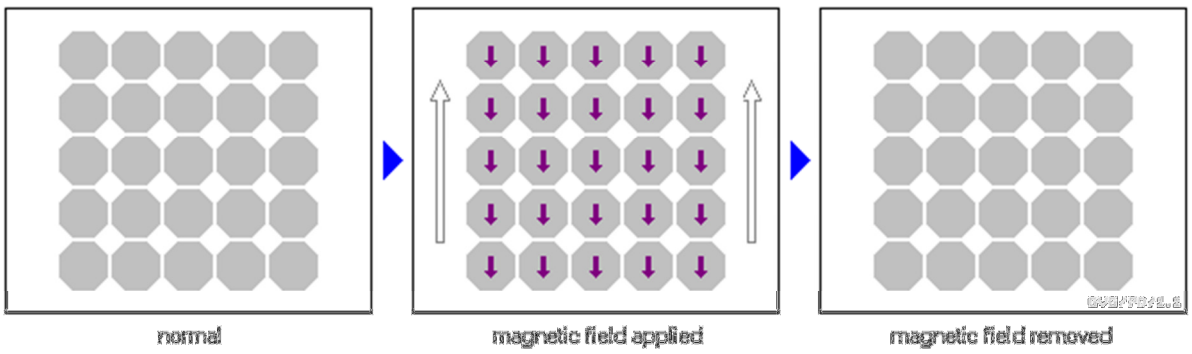

Fig 2.3: Schematic of the behavior of magnetic moments of a diamagnetic material

Paramagnetic materials have a net magnetic moment in the absence of an applied field. The magnetic moments tend to align in the direction of the applied force resulting in magnetization of the bulk material however, the material losses its magnetism in the absence of the field. Paramagnetic materials have a small and positive magnetic susceptibility also in the order 10^{-5} and $\mu_r \geq 1$. Some of these materials include Platinum, Tungsten, and Potassium. Conduction electrons have magnetic moments that result in Pauli Paramagnetic susceptibility of the material. The paramagnetic susceptibility of metals does not depend on tem perature whereas non-metallic materials do as stated by Curie's law [26]. From Langevin model of paramagnetic materials, increased thermal agitation of the materials is caused by temperature increases which also make it difficult to align the atomic magnetic moments and hence decrease in susceptibility [30]. This is given by the Curies Law as;

$$\chi = \frac{C}{T} \tag{2.51}$$

C and T are known as the Curie's constant and Curie's temperature respectively.

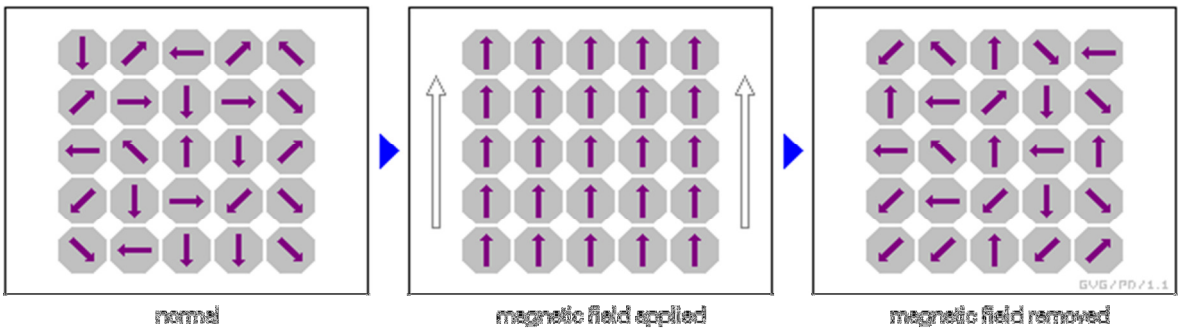

Fig 2.4: Schematic of the behavior of magnetic moments of a paramagnetic material

Ferromagnetic material show spontaneous magnetization and maintain their magnetism even in the absence of the applied field. These materials exhibits paramagnetism above a critical temperature and are usually characterized by saturated magnetization. As ferromagnetic materials are heated, the thermal agitation increases with decrease in the degree of alignment of atomic moments as a result saturation magnetization decreases until a critical temperature where the material becomes paramagnetic [30]. This temperature is known as the Curie's Temperature (T_c) and given by the Curie Weiss Law.

$$\chi = \frac{C}{T-\theta} \tag{2.52}$$

The microscopic origin of ferromagnetism is due to the Exchange Interaction between electrons and the dipole interaction between magnetic moments within the material as described by the Heisenberg model. As the temperature of the material is less than the Curie's Temperature ($T<T_c$), the exchange interaction dominates the thermal agitation hence spontaneous magnetization and when $T>T_c$ then, thermal agitation dominates with paramagnetism.

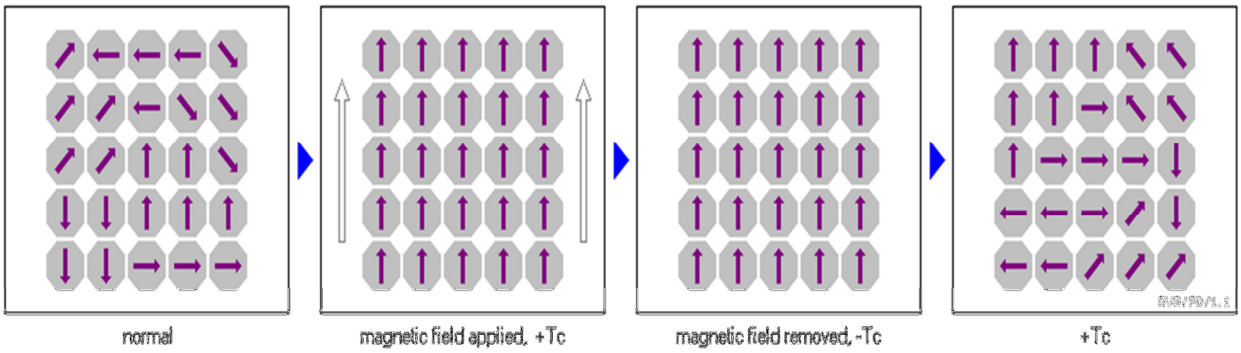

Fig 2.5: Schematic of the behavior of the magnetic moment of a ferromagnetic material

The type of ferromagnetic material depends on the size of the hysteresis loop or magnetization curve where materials with small coercive are termed Soft magnetic materials and easily magnetized. Those with large coercive are termed Hard materials and difficult to magnetize [24]. Examples of ferromagnetic material include Iron, Cobalt, Nickel, Gadolinium and Dysprosium.

Other magnetic materials include Antiferromagnetic and Ferrimagnetic materials. In Antiferromagnetic materials, the magnetic moments tend to align anti-parallel to each other and are of equal magnitude therefore there is no net magnetization in the absence of an applied field e.g. Cromium. Ferrimagnetic materials have anti-parallel magnetic moments but not of equal magnitude hence net magnetic moment in the absence of an applied field e.g. ferrites

2.6.1 MAGNETIC NANOPARTICLES

Contemporarily, magnetic nanoparticles have created exciting new opportunities including improving the quality of Magnetic Resonance Imaging (MRI), hyperthermia treatment of malignant cell, site-specific drug delivery and cell membrane manipulation [17]. According to Goya et al [23], most applications of magnetic nanoparticles (MNPs) at present are based on the following physical priniciples;

- The application of controlled magnetic field gradients around the desired location for remotely positioning MNPs in organs or tissues e.g. targeting, magnetic implants, and magnetic separation applied to the sequencing of DNA.
- The use of MNPs magnetic moment as a disturbance of the proton nuclear resonance e.g. contrasts media for Magnetic Resonance Imaging.
- Magnetic losses of nanometric particles in colloids for the purpose of heating e.g. magnetic hyperthermia.

The biomedical application of magnetic nanoparticles both *in vivo* and *in vitro* depends on the size, shape and to a large extend the surface chemistry of the particles. *In vitro* application of magnetic materials involves relatively large magnetic particles which maintain their magnetism even after the removal of the applied field. *In vitro* applications are mainly diagnostic either separation/selection or magnetorelaxometry. *In vivo* applications on the other hand use very small sized particles in the range of 10-100nm, and exhibit paramagnetism in the absence of the

applied field. *In vivo* applications are both therapeutic (hyperthermia and drug targeting) and diagnostic (Nuclear Magnetic Resonance, NMR) [15].

In *in vivo* application however, the magnetic particles must prove to be biocompatible, stable and biodegradable which is achieved by coating and embedding the particles in suitable materials [31]. Most commonly used surfactant are polysaccharides like dextran or polymers such as polyvinyl alcohol used for coatings and other water-based ferrofluids.

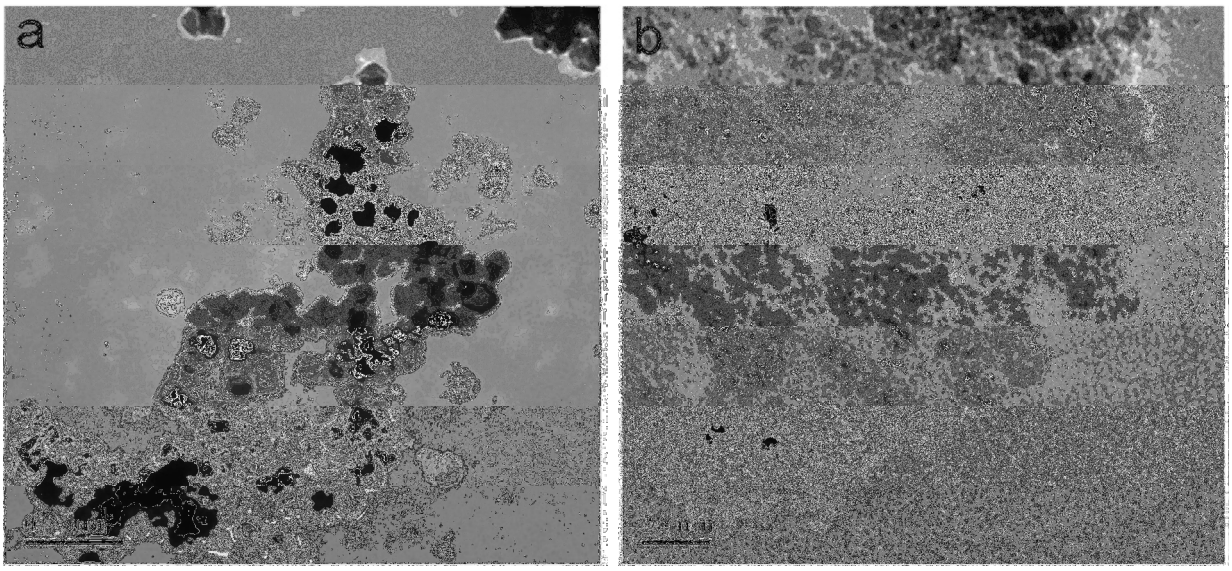

Fig 2.6: TEM images of magnetite nanoparticles (a) Uncoated, (b) Dextran coated [32]

Encapsulating the magnetic particles also allow possible modification of their surface by attaching bioactive components such as antibodies, protein, biotin, carboxyl groups etc. broadening their applications [31].

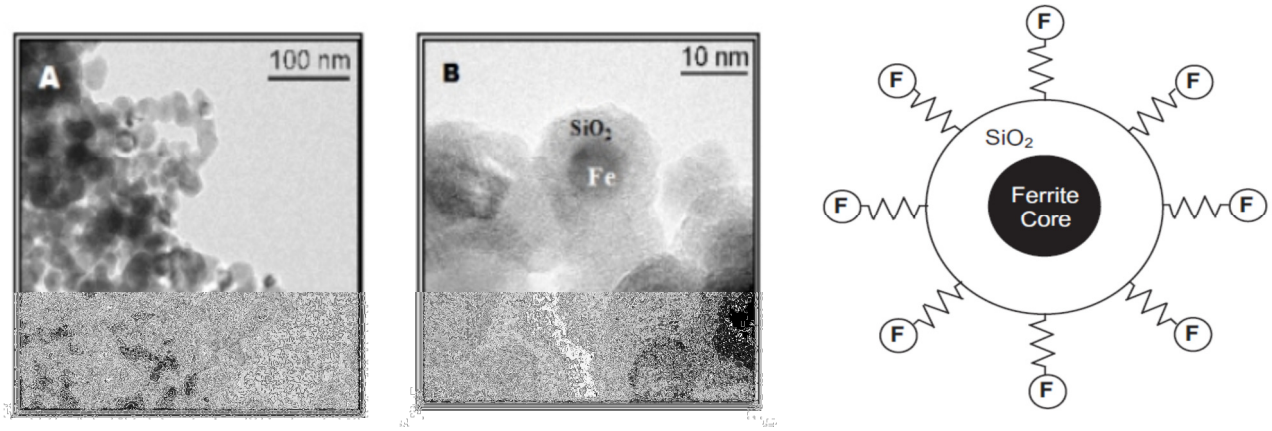

(i) (ii)

Fig 2.7: (i) TEM images of Silica coated iron nanoparticles [23], (ii) Schematic of a functionalized magnetic nanoparticle core of ferrite with a silica shell and functional groups attached to the shell [18]

The use of magnetic materials in hyperthermia was first proposed by Gilchrist et al [33] in 1957 where magnetic microspheres where introduced into tissues of animals and an applied alternating magnetic field. The alternating field result in the reorientation of the magnetic moments of the material and due to the interaction between the magnetic moments of the particles and the field, energy is converted to thermal energy for therapeutic purposes.

Nanoparticle are therefore being investigated for preferential heating of biological structures for cancer treatment where electromagnetic energy is intended to cause localized heating of nanoparticles attached to cancer cells or embedded in tumors resulting in selective destruction of the diseased tissues [34].

Magnetite (Fe_3O_4) and maghemite (γ-Fe_2O_3) which are composed of Iron oxide are identified among other magnetic materials as potential heating agents in biological tissues due to their biocompatibility. Their different sizes, surfactant coating and heating effects with various AC magnetic fields have been investigated [32].

CHAPTER THREE

THEORETICAL AND COMPUTATIONAL MODELS

3.1 MAGNETIC NANOPARTICLE HEATING WITH ALTERNATING MAGNETIC FIELD

In the presence of an alternating magnetic field, magnetic particles are able to generate heat based on hysteresis losses, relaxation losses, resonance losses or eddy currents. The heat generated is dependent on the size and magnetic properties of the magnetic material. It is therefore essential to consider the parameters that will optimize the heat generation including the intensity and frequency of the applied field. This section puts to light the underlying physical mechanisms by which the nanoparticles generate heat in the device.

3.1.1 CONSERVATION OF ENERGY IN ELECTROMAGNETIC FIELDS

The law of conservation of energy otherwise known as the Poynting Theorem is the basic principle governing energy conservation in electromagnetic fields. The Poynting vector which is found to be the Power Intensity of the electromagnetic field is defined to be the cross product of the Electric field and Magnetic field Intensities. The Poynting vector is given as;

$$\vec{P} = \vec{E} \times \vec{H} \tag{3.0}$$

To derive the Poynting theorem, we consider the Maxwell's equations, Gauss divergence theorem and vector analysis. Consider the field to be homogeneous, linear and isotropic region or volume bounded by a closed surface S with power sources.

From the Maxwell's equations;

$$\nabla \times \vec{E} = -\frac{\partial \vec{B}}{\partial t} \tag{3.1}$$

$$\nabla \times \vec{H} = \vec{J} + \frac{\partial \vec{D}}{\partial t} \tag{3.2}$$

The power into the closed volume is given as the negative of the surface integral over the volume.

$$\mathcal{P} = -\oint_S \vec{E} \times \vec{H}\, d\vec{s} \tag{3.3}$$

From Gauss's Divergence theorem

$$\mathcal{P} = -\oint_V \nabla \cdot \left(\vec{E} \times \vec{H}\right) d \tag{3.4}$$

In addition, the identity from vector calculus has it that

$$\nabla \cdot \left(\vec{E} \times \vec{H}\right) = \vec{H} \cdot \left(\nabla \times \vec{E}\right) - \vec{E} \cdot \left(\nabla \times \vec{H}\right) \tag{3.5}$$

$$\mathcal{P} = \oint_V \vec{E} \cdot \left(\nabla \times \vec{H}\right) dV + \oint_V \vec{H} \cdot \left(-\nabla \times \vec{E}\right) dV \tag{3.6}$$

$$\mathcal{P} = \oint_V \vec{E} \cdot \vec{J} dV + \oint_V \vec{E} \cdot \frac{\partial \vec{D}}{\partial t} dV + \oint_V \vec{H} \cdot \frac{\partial \vec{B}}{\partial t} dV \tag{3.7}$$

Due to isotropy of the material such that

$$\vec{D} = \varepsilon \vec{E} \qquad \vec{B} = \mu \vec{H}$$

$$\mathcal{P} = \oint_V \vec{E} \cdot \vec{J} dV + \oint_V \vec{E} \cdot \varepsilon \frac{\partial \vec{E}}{\partial t} dV + \oint_V \vec{H} \cdot \mu \frac{\partial \vec{H}}{\partial t} dV \tag{3.8}$$

$$\mathcal{P} = \oint_V \vec{E} \cdot \vec{J} dV + \frac{d}{dt} \oint_V \left(\frac{1}{2} \varepsilon |E|^2 + \frac{1}{2} \mu |H|^2\right) dV \tag{3.9}$$

The conservation of energy therefore shows that the power into a volume from an electromagnetic field is equal to the sum of the stored electromagnetic energy that is both Electric and Magnetic energy and the heat dissipated in the volume.

Heat Dissipated $$U_{dis} = \oint_V \vec{E} \cdot \vec{J} dV = \oint_V \sigma \vec{E} dV \tag{3.10}$$

Electric Energy stored $$U_e = \oint_V \frac{1}{2} \varepsilon \frac{\partial |E|^2}{\partial t} dV \tag{3.11}$$

Electric Energy stored $$U_m = \oint_V \frac{1}{2} \mu \frac{\partial |H|^2}{\partial t} dV \tag{3.12}$$

where the Electric and Magnetic energy densities are $U_{ev} = \frac{1}{2} \vec{D} \cdot \vec{E}$ and $U_{mv} = \frac{1}{2} \vec{B} \cdot \vec{H}$ respectively.

3.1.2 SPECIFIC ABSORPTION RATE (SAR) OF NANOPARTICLES

It is the measure of the rate at which energy is absorbed by the magnetic nanoparticles and measured in W/kg. The maximization of Specific Absorption Rate of magnetic nanoparticles used in hyperthermia is of great importance since it reduces tissue-loading or allows reduction of ferrofluid dose in in vivo. SAR can be obtained experimentally by calorimetric measurements. From the measured temperature rates, SAR is calculated by;

$$SAR = C_s \frac{\Delta T}{\Delta t} \tag{3.13}$$

C_s is the samples heat capacity defined as mass-weighted mean value for a given concentration of magnetic materials.

$$C_s = \frac{m_{Fe}C_{Fe}+m_l C_l}{m_{Fe}+m_l} \tag{3.14}$$

C_{Fe}, m_{Fe} and C_l, m_l are the heat capacities and masses of the magnetic material and liquid carrier respectively.

$\Delta T/\Delta t$ is the slope of the time-dependent temperature curve or temperature rate.

SAR is dependent on the viscosity of the ferrofluid, the amplitude and frequency of the AC field and particle size. According to Skumiel et al [35] in their experiment of studying the suitability of ferrofluids composed of $CoFe_3O_4$ for biological applications, testified to the H^2- Law type dependence of the SAR on the amplitude of the field at frequencies 600-800 KHz and superparamagnetism behavior of the particles.

The heating power of magnetic nanoparticles in magnetic fluid hyperthermia is quantified by the SAR. The heat generated by the particles is therefore the product of the density of the particles and the SAR.

$$P = SAR \times \rho \tag{3.15}$$

3.2 HEAT DISSIPATION

In magnetic fluid hyperthermia, magnetic nanoparticles dissipate energy through hysteresis losses, relaxation losses and resonance losses or eddy currents. These mechanisms are dependent on the size and material parameters of the nanoparticles. For the purpose of hyperthermia, resonance losses can be ignored since it occurs at very high frequencies. Also, eddy currents heating is considered negligible due to the particles small size. Hysteresis properties of the nanoparticle determine the hysteresis losses and can be obtained from the hysteresis loop considering the power and frequency of the alternating field [32].

It is proven that in an alternating field, large size of magnetic multidomain particles leads to hysteresis loss induced heating whereas small size particles with single domain structure result in induced heating by relaxation losses [16].

For a constant density system of volume, the first law of thermodynamics has it that

$$dU = \delta Q + \delta W \tag{3.16}$$

U is Internal energy of the system, Q is heat added and W the magnetic work done.

Since the device and its immediate surrounding can be considered to be undergo an adiabatic process, then $\delta Q = 0$;

$$dU = \delta W \tag{3.17}$$

Differential magnetic work is given as;

$$\delta W = \vec{H} d\vec{B} \tag{3.18}$$

$$dU = \vec{H} d\vec{B} \tag{3.19}$$

$\vec{H}$ is the magnetic field intensity (A/m) and $\vec{B}$ the magnetic induction (T).

Also, $$\vec{B} = \mu_o(\vec{H} + \vec{M}) \tag{3.20}$$

Where M is the magnetization, $\mu_o = 4\pi \times 10^{-7}$ (TmA^{-1}) is the permeability of free space.

Substituting (3.20) into (3.19) and integrating by part, the results show the cyclic increase in the internal energy.

$$\Delta U = -\mu_o \oint \vec{M} d\vec{H} \tag{3.21}$$

When magnetization lags the field, the integration above yields a positive result indicating conservation of magnetic work to internal energy. In writing the magnetization in terms of a complex ferrofluid susceptibility

$$\chi = \chi' - i\chi'' \tag{3.22}$$

Then with an applied magnetic field of the form

$$H(t) = H_o Cos\omega t = Re\ (H_o e^{i\omega t}) \tag{3.23}$$

The resulting magnetization

$$M(t) = Re[\chi H_o e^{i\omega t}] = H_o(\chi' Cos\omega t + \chi'' Sin\omega t) \tag{3.24}$$

It is clear that χ' is in-phase component and χ'' is out-of-phase component of χ.

Substituting the magnetization and magnetic field into (3.21) we obtain

$$\Delta U = 2\mu_o H_o^2 \chi'' \int_0^{2\pi/\omega} Sin^2\ \omega t dt \tag{3.25}$$

χ'' in the equation is known as the loss component or heat generation.

Integrating equation (3.25) and multiplying by the cyclic frequency of $f = \omega/2\pi$, we obtain the volumetric heat dissipation of the system.

$$P = f\Delta U = \ \mu_o \pi \chi'' f H_o^2 \tag{3.26}$$

Hence, χ'' is related to the material parameter of the ferrofliud.

3.2.1 THEORY OF HEATING WITH TIME DEPENDANT MATERIAL PARAMETER

For a single domain magnetic material in a time-varying magnetic field, the magnetization is also time variant. Therefore, the time derivate of a magnetic fluid in an oscillating field is given as [36].

$$\frac{\partial M(t)}{\partial t} = \frac{1}{\tau}\left(M_o(t) - M(t)\right) \tag{3.27}$$

$$M_o(t) = Re[\chi_o H_o e^{i\omega t}] = \chi_o H_o Cos\omega t \tag{3.28}$$

M_o is equilibrium magnetization, χ_o is static/equilibrium susceptibility, τ is characteristic relaxation time.

In order to determine the effect of the relaxation mechanisms, the frequency dependence of the susceptibility can be written as;

$$\chi(\omega) = \frac{\chi_o}{1+(\omega\tau)^2} - i\frac{\chi_o\,\tau}{1+(\omega\tau)^2} \tag{3.29}$$

The components of the susceptibility are therefore given as;

$$\chi' = \frac{\chi_o}{1+(\omega\tau)^2} \tag{3.30}$$

$$\chi'' = \frac{\omega\tau}{1+(\omega\tau)^2}\chi_o \tag{3.31}$$

The above equations are similar to the Debye spectra of polar molecules in the absences of a constant field [36].

3.2.2 RELAXATION MECHANISMS

In the absence of an applied magnetic field, the magnetization of the ferrofluid relaxes back to zero due to the ambient thermal energy of its environment. The relaxation is either due to the physical rotation of the particles within the fluid or rotation of the atomic magnetic moments within each particle [18]. In this model of heating, we consider single-domain magnetic nanoparticles which are not interactive with each other and have fixed magnetic moment. The two relaxation mechanisms that result in heat generation are the Brownian and Néel relaxations. Brownian relaxation occurs due to the whole rotation of the particles in alignment to the field

and Néel relaxation is due to the changing direction of the magnetic moments inside the particles. These mechanisms are characterized by relaxation times.

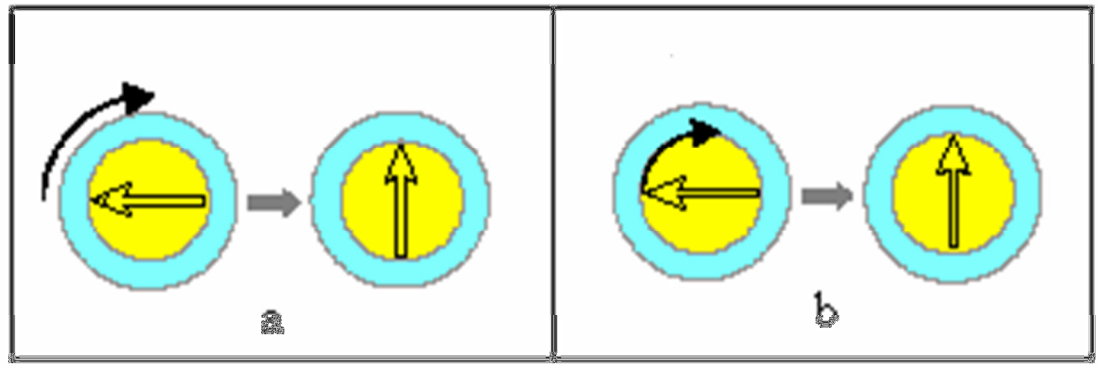

Fig 3.0: Relaxation mechanisms of MNP's: a- Brownian Relaxation, b- Néel Relaxation. Structure of MNP: yellow (core), Blue (shell), arrow represent direction of magnetization [13].

Brownian relaxation time τ_B is dependent on the hydrodynamic properties of the fluid and temperature.

$$\tau_B = \frac{3\eta V_H}{K_B T} \tag{3.32}$$

η is viscosity of the matrix fluid, K_B the Boltzmann constant, T absolute temperature and V_H the particle volume including the surfactant layer or hydrodynamic volume.

$$V_H = \left(1 + {}^{\delta}/_{r}\right)^3 V_m \tag{3.33}$$

$$V_m = \frac{4}{3}\pi r^3 \tag{3.34}$$

V_m is the nanoparticle core volume, r the nanoparticle radius and δ the thickness of the surfactant layer.

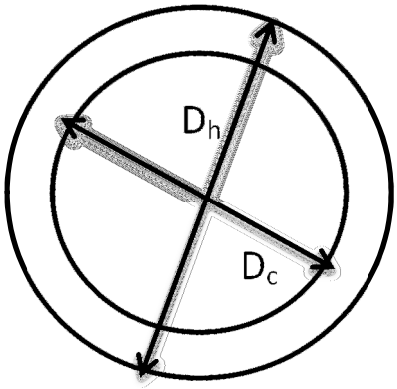

Fig 3.1: Magnetic and Hydrodynamic diameter of a nanoparticle with surfactant layer [37]

Both the Brownian and Néel relaxation times are a function of the nanoparticle diameter [37]. Néel relaxation time is given as;

$$\tau_N = f_o^{-1} \exp\left(\frac{K_a V_m}{K_B T}\right) \tag{3.35}$$

Or equivalently

$$\tau_N = \frac{\sqrt{\pi}}{2} \tau_D \frac{\exp \Gamma}{\Gamma^{3/2}} \tag{3.36}$$

$$\Gamma = \frac{K_a V_m}{K_B T} \tag{3.37}$$

$$\tau_D = \Gamma \tau_o \tag{3.38}$$

Where f_o is lamour frequency of the magnetic moments, $f_o^{-1} = \tau_o$, K_a is the anisotropy constant of the nanoparticles.

A typical ferrofluid has broad distribution of particle size with mean size ~ 10nm. The effective relaxation time τ is given as;

$$\frac{1}{\tau} = \frac{1}{\tau_B} + \frac{1}{\tau_N} \tag{3.39}$$

For small nanoparticle size, Néel relaxation time constant dominate whereas Brownian relaxation time for large size particles. However, to achieve high heating rates, the Néel relaxation must not be allowed to dominate [36]. The figure below shows that shorter time constants dominate in determining the effective relaxation time for a given particle size.

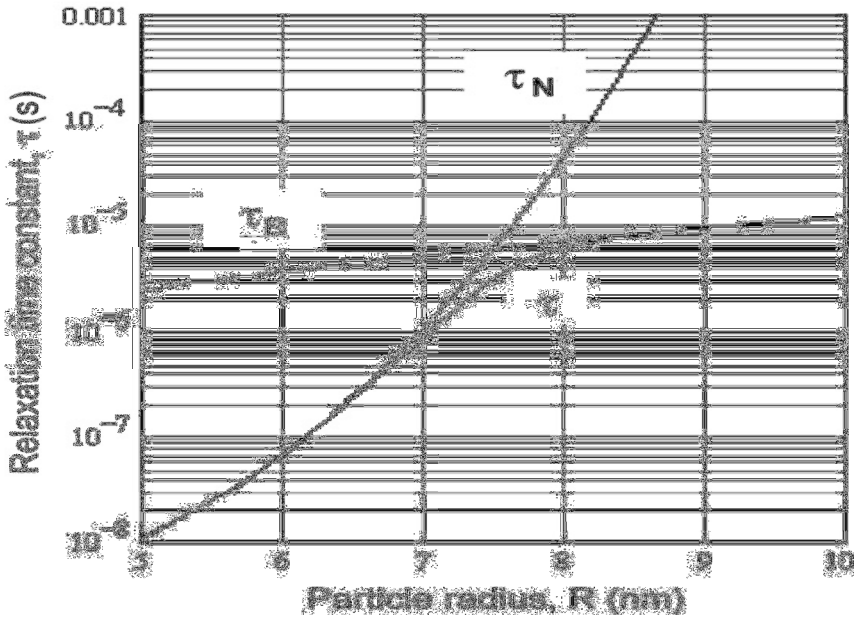

Fig 3.2: Time constant against particle size for magnetite particles [36]

From equation (3.31) and substituting χ'' into equation (3.26), the power dissipation is expressed as;

$$P = \mu_o \pi \chi_o H_o^2 f \frac{\omega\tau}{1+(\omega\tau)^2} \tag{3.40}$$

where $\omega = 2\pi f$

$$P = \mu_o \pi \chi_o H_o^2 f \frac{2\pi f\tau}{1+(2\pi f\tau)^2} \tag{3.41}$$

Equation (3.41) is the expression for a monodispersion power dissipation density assuming the susceptibility is constant. The equilibrium susceptibility χ_o is dependent on the magnetic field and assumed to be the chord susceptibility of Langevin equation.

$$L(\xi) = \frac{M}{M_s} = \coth\xi - \frac{1}{\xi} \tag{3.42}$$

$$\xi = \frac{\mu_o M_d H V_m}{KT} \tag{3.43}$$

$$H = H_o \mathrm{Cos} 2\pi f t \tag{3.44}$$

The Langevin parameter is ξ whereas M_s is the saturation magnetization of the ferrofliud;

$$M_s = \phi M_d \tag{3.45}$$

M_d is the domain magnetization of the suspended nanoparticles and ϕ is the volume fraction of the nanoparticles or concentration. The equilibrium or static susceptibility is given as;

$$\chi_o = \chi_i \frac{3}{\xi}\left(\coth\xi - \frac{1}{\xi}\right) \tag{3.46}$$

χ_i is the initial susceptibility and defined as;

$$\chi_i = \left(\frac{\partial M}{\partial H}\right)_i = \frac{\mu_o \phi M_d^2 V_m}{3KT} \tag{3.47}$$

The Specific Loss Power (SLP) for a monodisperse particle solution can be evaluated by;

$$SLP = \frac{P}{\rho\phi} = \frac{1}{\rho\phi}\mu_o \pi \chi_o H_o^2 f \frac{\omega\tau}{1+(\omega\tau)^2} \quad (3.48)$$

ρ is the mass per unit volume of the nanoparticles.

The temperature rise of the ferrofluid is calculated;

$$\Delta T = \frac{P\Delta t}{C} \quad (3.49)$$

C is the specific heat capacity of the ferrofluid, Δt is the duration of the heating.

The specific heat capacity is computed as;

$$C = \rho C_p \quad (3.50)$$

$$\rho = \phi\rho_n + (1-\phi)\rho_m \quad (3.51)$$

$$C_p = \phi C_{pn} + (1-\phi)C_{pm} \quad (3.52)$$

C_p and ρ are the specific heat and effective density respectively. Also the subscripts n and m represent nanoparticles and medium respectively.

3.3 MODELLING MAGNETIC FLUID HYPERTHERMIA IN AN IMPLANTABLE DEVICE

In hyperthermia treatment of cancer, it is important to estimate the amount of heat required for temperature distribution within the normal and diseased tissue, hence the need to model the thermal behavior of the implantable device and its environment.

In this research, the geometry of the device and its environment is modeled such that it is incorporated into finite element software known as Abaqus/CAE 6.9 in order to calculate the heat diffusion profile from the implant to its environment. The implant is modeled as rectangular shaped with $1cm^2$ area. The device and its immediate environment is modeled to have an area of $10cm^2$ that occupies between 800 and 1000 nodes being the maximum nodes allowed for this version of the software. The area close to the device is considered the diseased tissue whereas that very far and close to the boundary being normal tissue.

Abaqus/CAE 6.9 solves the heat conduction of the implant based on finite element discretization, boundary conditions, time integration among other procedures. The heat conduction is governed by Fourier's law. Abaqus use backward difference algorithm and an automatic (self adaptive)

time stepping algorithm to choose time increment as well as user defined maximum temperature changed allowed in each time increment and convergence rate.

The heat generated by the nanoparticles in the PDMS is inculcated into the initial step of the Abaqus procedure which is set to steady state temperature in the given exposure time of the field. This is seen as the heating step for the device. The maximum temperature of the heat generated is then used as the boundary condition for the wall of the implant or PDMS casing. This temperature was varied between 45^{o}C and 52^{o}C whereas the boundary of the environment of the implant was set at normal body temperature of 37^{o}C creating a gradient for heat flow. The heat conduction step is then set to transient response where the heat transfer flow to steady state at longer time scales.

3.4 FINITE ELEMENT METHOD

Many physical phenomena in engineering and science can be described in terms of Partial Differential Equations (PDE's). In general, solving these equations by classical analytical methods is almost impossible since engineering and physics problems are not simple in nature. This is particularly seen in the case where PDE's are nonlinear, complex solution regions, fixed typed and time dependent boundary conditions as well as anisotropic media. In the 1920s, A. Thom et al [38] developed the first Finite Difference Method (FDM) for solving nonlinear hydrodynamic equations under the title "the method of squares".

Finite difference technique is based upon approximations that replace differential equations with finite difference equations. FDM involves dividing the solution into grids of nodes, replacing the differential equations with finite difference equations that relate the solution to the grid points and solving the difference equations based on boundary or initial conditions.

For irregular geometries and unusual specifications of boundary conditions however, there is difficulty in using FDM and therefore the development of Finite Element Method (FEM) which essentially give a consistent technique for modeling the domain as a whole or geometry as an assembly of discrete parts [19].

Finite Element Method (FEM) is a numerical approach to solving differential or integral equations approximately. The method essentially consist of assuming the piecewise continuous function of the solution and obtaining the parameters of the function in a way that reduces the error in the solution. This method was used in the early 1960s by engineers to solve problems in stress analysis, heat transfer, and fluid flow among others and now widely used in diverse field to solve static and dynamic problems including fluid mechanic, electromagnetics, biomechanics, structure analysis, mechanical/aerospace/civil engineering, geomechanics, etc.

FEM uses a step by step procedure in solving the PDE's. The basic steps in FEM include discretizing the continuum, selecting the interpolation function, finding the element properties, assembling the element properties, impose boundary condition, solving the system equations and post processing the results.

Finite Element Method and or Finite Element Analysis (FEA) are the most widely used computer simulation method in engineering. In computer implementation of FEM, three basic processes are involved being preprocessing, FEA solver and post processing. Preprocessing consist of building the finite element model or geometry, imposing loads and constraints or boundary conditions. The FEA solver assembles and solves the system of equations generated by the model. Post processing sorts and display the desired results. There exist several FEM software packages for engineering simulation some of which include ANSYS, NASTRAN, ABAQUS, and COSMOS.

In this research, ABAQUS/CAE 6.9 student version was used for the finite element modeling and simulation. The package presents an environment for creating Abaqus models, interactively submitting and monitoring Abaqus jobs and evaluating results from Abaqus simulations. Abaqus/CAE is divided into modules each defining the logical process of modeling e.g. defining the geometry, material properties, and mesh. After completing all the modules, Abaqus/CAE generates an impute file that is submitted to Abaqus analysis product which perform analysis and generates an output database. Result of the simulation is then viewed from the output database.

CHAPTER FOUR

RESULTS AND DISCUSSION

4.1 NUMERICAL MODELING

In order to obtain the temperature rise of the polydimethylsiloxane (PDMS) and nanoparticle matrix, MATLAB codes were written to solve the numerical equations governing the heat generation. According to the mathematical models on heat dissipation and temperature rise, there is strong dependence of the temperature rise on the material properties of the matrix, magnetic properties of the nanoparticles, and the properties of the applied field. The temperature rise is therefore, a function of several parameters including frequency (f), amplitude of the field (H_o), relaxation time (τ), volume fraction of the nanoparticles, viscosity of the PDMS (η), and static or equilibrium susceptibility (χ_o) some of which are interrelated and implicit.

For instance, the static susceptibility of the nanoparticles is a function of the Langevin parameter which in turn is a function of the amplitude of the field. The viscosity of the PDMS is also a directly proportional to the Brownian relaxation time and consequently the effective relaxation time. Consideration is given to those parameters that dominant in terms of the temperature rise. Below is a table showing some of the parameters used in the computation.

Table 4.0: Parameters for heat generation computation

Parameter	Measure	SI Unit
Larmour frequency (τ_o)	10^{-9}	s
Boltzmann constant (K_B)	1.38×10^{-23}	JK^{-1}
Absolute temperature (T)	310	K
Anisotropy factor (K_a)	23×10^3	Jm^{-3}
Domain magnetization (M_d)	414×10^3	Am^{-1}
Specific heat of nanoparticles (C_{p1})	670	$Jkg^{-1}K^{-1}$
Specific heat of PDMS (C_{p2})	1350	$Jkg^{-1}K^{-1}$
Density of nanoparticles (ρ_1)	5180	Kgm^{-3}
Density of PDMS (ρ_2)	970	Kgm^{-3}
Amplitude of field (H_o)	$5 – 11.93 \times 10^3$	Am^{-1}
Frequency of field (f)	$8 – 27.8 \times 10^3$	Hz
Viscosity of PDMS (η)	$0.5 – 1.49 \times 10^{-3}$	Pa.s
Volume fraction (ϕ)	0.001 – 0.15	dimensionless

Some of the parameters where initially fixed while varying others so as to clearly see their dependence and to enable the informed design and selection of conditions that could enhance the performance of the device that are being developed for hyperthermia treatment of cancer cells and tissues.

Figure 4.0 below shows the effect of frequency and amplitude of the field on the temperature rise of the matrix.

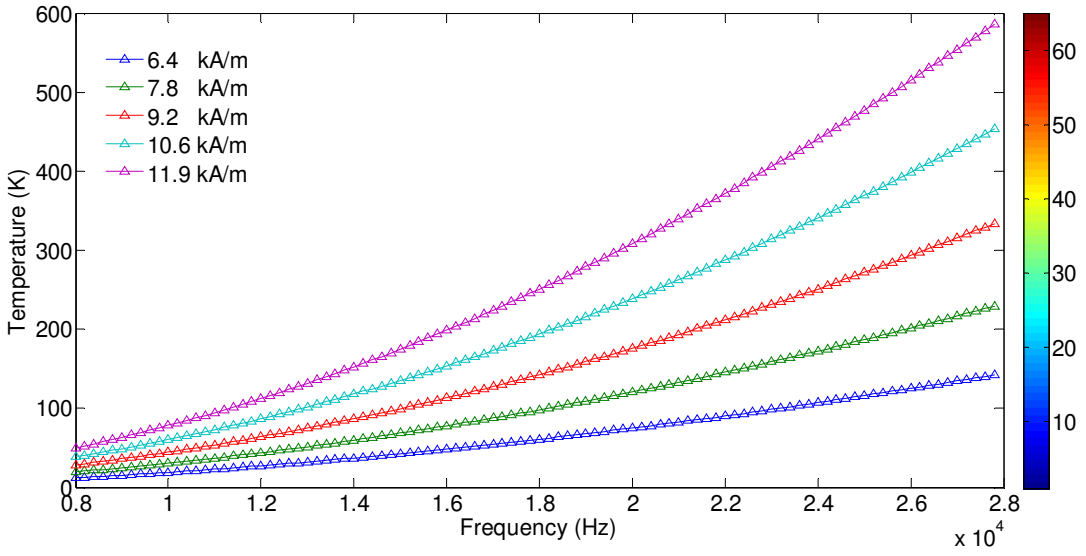

Fig 4.0: The temperature rise of the matrix against frequency for different field amplitudes

The graph generally shows a trend of increasing temperature with increasing frequency. Also, it is seen that for increased field amplitude, the initial and final temperatures increases. This confirms the fact that the temperature rise is directly and explicitly dependent on the frequency and amplitude of the field as predicted by the mathematical model.

The mesh plot of the frequency and amplitude of the field against the temperature rise in figure 4.1 below provides the intersection of the two parameters with regards temperature increase. It is, therefore, desirable to increase both the frequency and amplitude of the field since that rapidly yields high temperature.

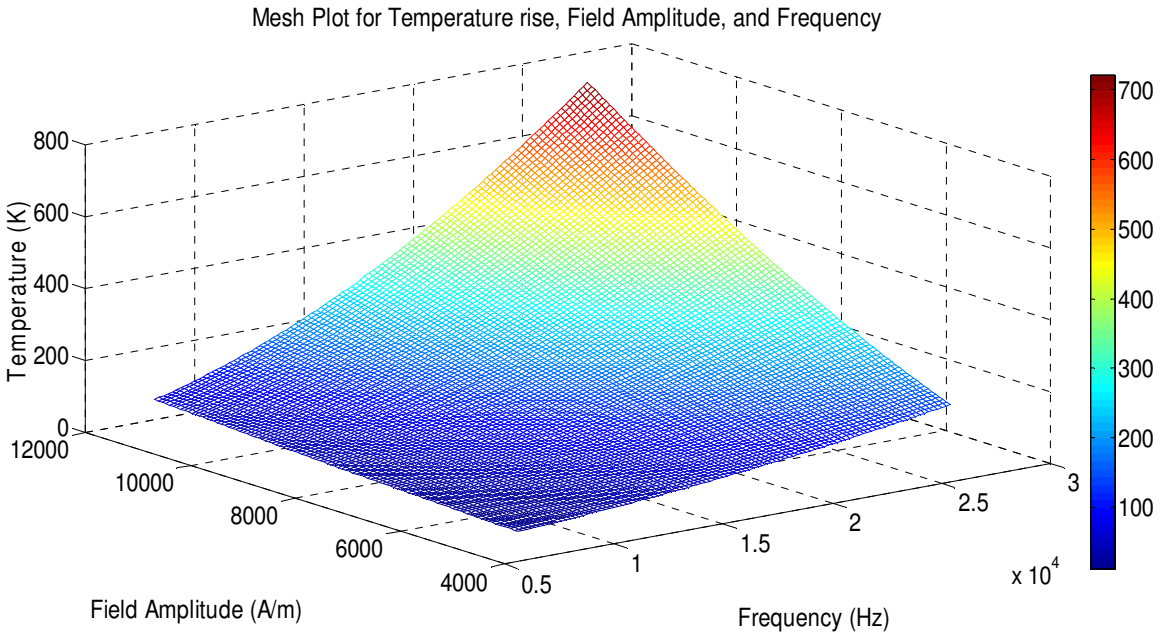

Fig 4.1: Mesh plot of Temperature rise, field amplitude and frequency of the field

In hyperthermia, the therapeutic temperature is identified to be 42°C. This corresponds to the therapeutic regime of 315K and above. The heat generated by the nanoparticle should be enough to raise the temperature to this amount based on the allowable frequencies and amplitude of the field.

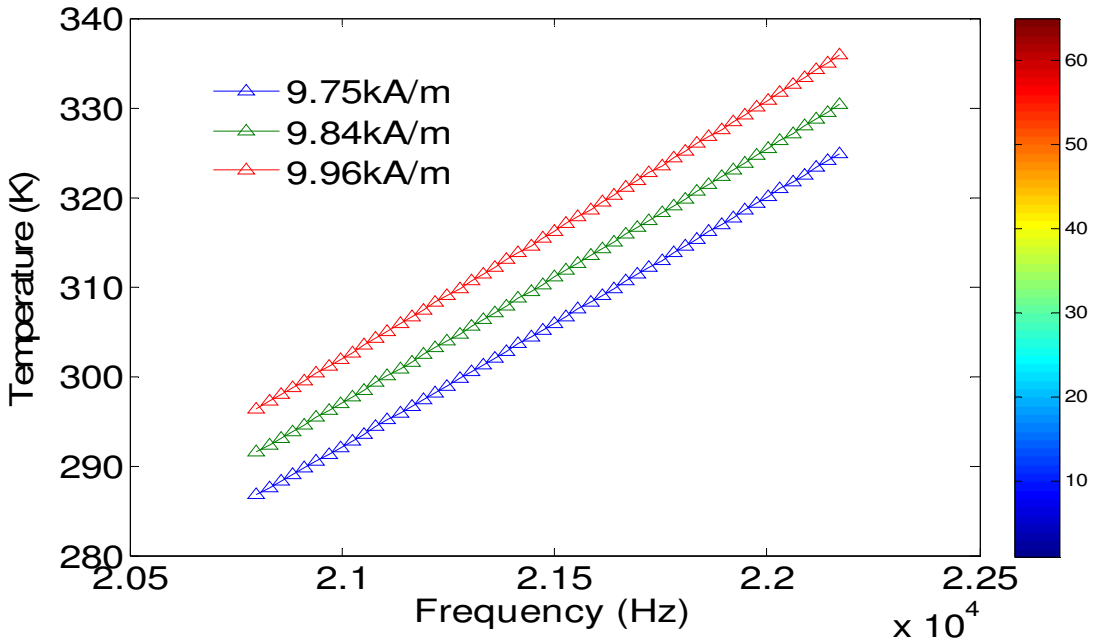

Fig 4.2: Therapeutic temperature range against frequency for different field amplitudes

From the numerical results of the computation, a frequency range of 21.6 – 21.9 kHz and a field amplitude of 9.77 – 9.89 kA/m yields temperatures between 37^{o}C and 54^{o}C. This is clearly seen in figure 4.2 above. According to Pankhurst et al [18], the usable range of frequencies and amplitude is considered to be 0.05-1.2MHz and 0-15kA/m respectively. The field amplitude of the numerical computation falls within this range but rather shows a relatively smaller frequency range. The higher frequency fields where rather used by Atkinson et al [39] who developed implantable metal thermoseeds for hyperthermia based on eddy current heating. In this research heating is based on relaxation losses rather than eddy current heating due to the small size of the nanoparticles accounting for the lower frequency range.

The experimental research of Atkinson et al [39] also concluded that exposure to fields where the product of the amplitude and frequency does not exceed 4.85 x 10^{8} $Am^{-1}s^{-1}$ is safe and tolerable. The product of the highest value of the amplitude and frequency from the computation is 2.19 x 10^{8} $Am^{-1}s^{-1}$ which is approximately half the predicted safe value.

The exposure time of the ferrite magnetic nanoparticles to the field at a given frequency and amplitude also showed increase in temperature with increasing time. This also satisfies the mathematical model that shows the direct proportionality of the temperature rise with exposure time and is seen in the plot below.

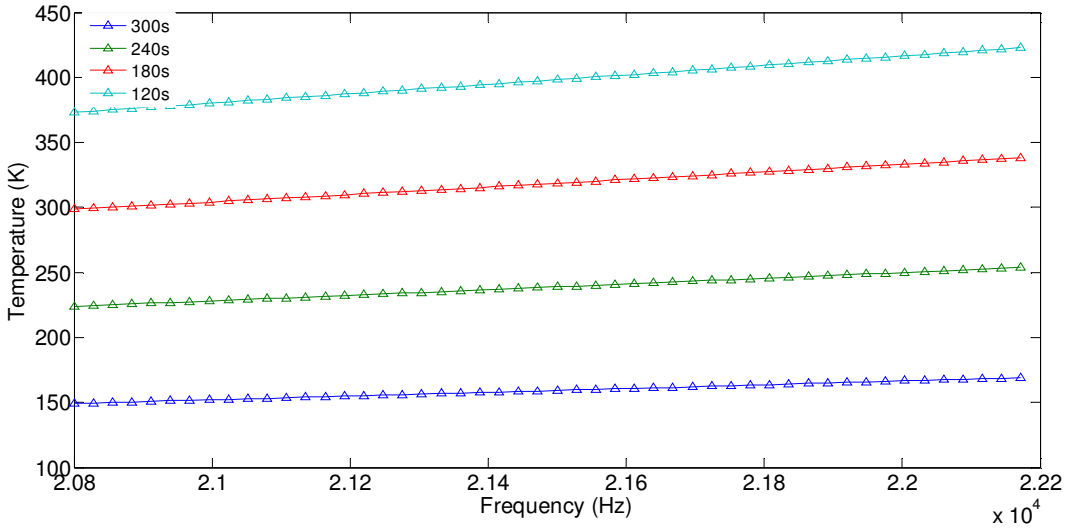

Fig 4.3: Temperature rise against frequency for different exposure time at fixed field amplitude of 9.98 kA/m

From the plots shown in Fig 4.3, an exposure time of 240s or three minutes will yield temperature close to the therapeutic temperature since all others will fall below or above the required range of temperatures. Hence, maintaining the exposure time at this value while altering other parameters will be useful.

The effect of the viscosity of the PDMS gel and volume fraction of the nanoparticle on the temperature rise is also made evident in the numerical results. As mentioned earlier, the viscosity is associated with the Brownian relaxation. The graph below shows it influence on the temperature rise.

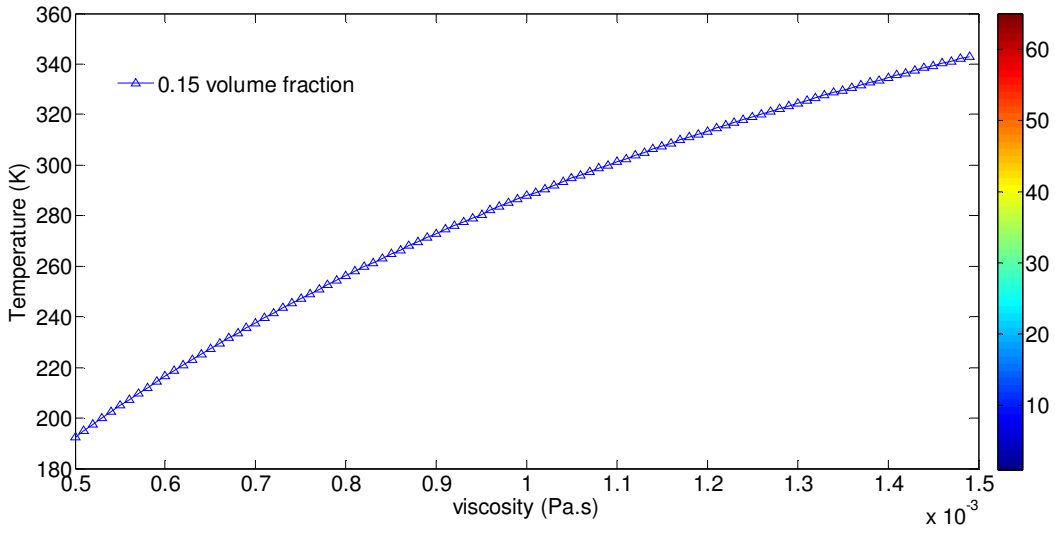

Fig 4.4: The effect of increasing viscosity on the temperature rise at fixed volume fraction of 0.15

The plot shows that increasing viscosity result in increasing temperature. It can be observed that the hyperthermia therapeutic temperature range occurs at viscosities between 1.1 and 1.2mPa.s. The trend of the influence of the viscosity on temperature is also in agreement with experimental results as conducted by Li Yung et al [32] on magnetic ferrofluid with high Specific Absorption Rate (SAR) for hyperthermia. Their result revealed that SAR of dextran-coated magnetite nanoparticles increased with increasing viscosity with the maximum occurring at 1.96mPa.s.

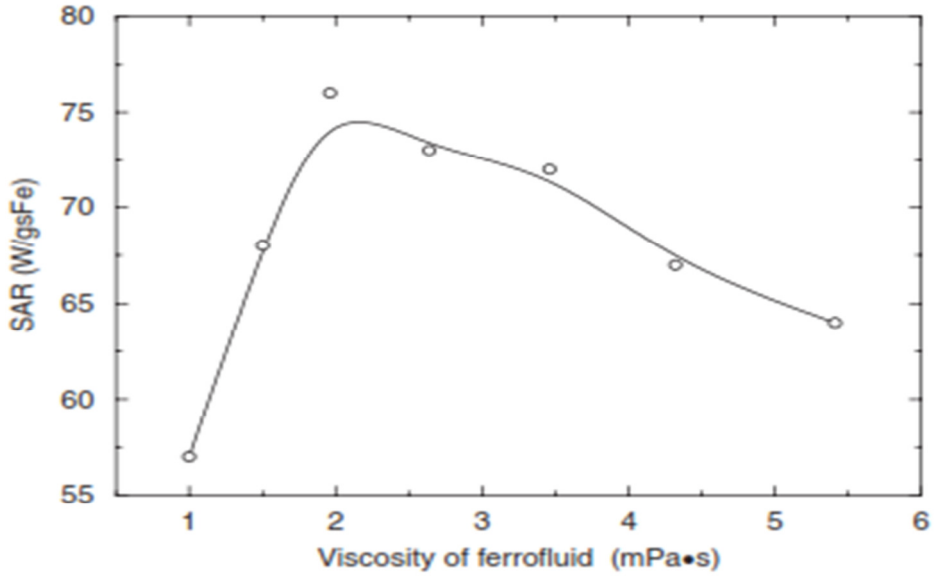

Fig 4.5: The SAR of dextran-coated magnetite ferrofluid measured calorimetrically in dependence on the viscosity of the fluid [32]

This is in agreement with the numerical results of computation because the Specific Absorption Rate (SAR) is directly proportional to the heat generated or power density of the nanoparticles and due to the fact that the temperature rise is also directly proportional to the power density. Additionally, the maximum value of the viscosity in the computation is less than the maximum, as shown by their results. Hence the maximum temperature rise cannot be observed in Fig 4.4.

The dependence of the temperature rise on the volume fraction of the nanoparticles is also seen to confirm what is in literature. In increasing the dose of nanoparticles will increase the total amount of heat generated, hence higher temperature rise as desired. This is in accordance with Oyku experimental finding that the temperature increase can be approximated to linear relationship with concentration of nanoparticles. However, the concentration must not exceed 55mg/ml since beyond this value heating rate drops significantly. This is due to agglomeration at high concentrations of nanoparticles.

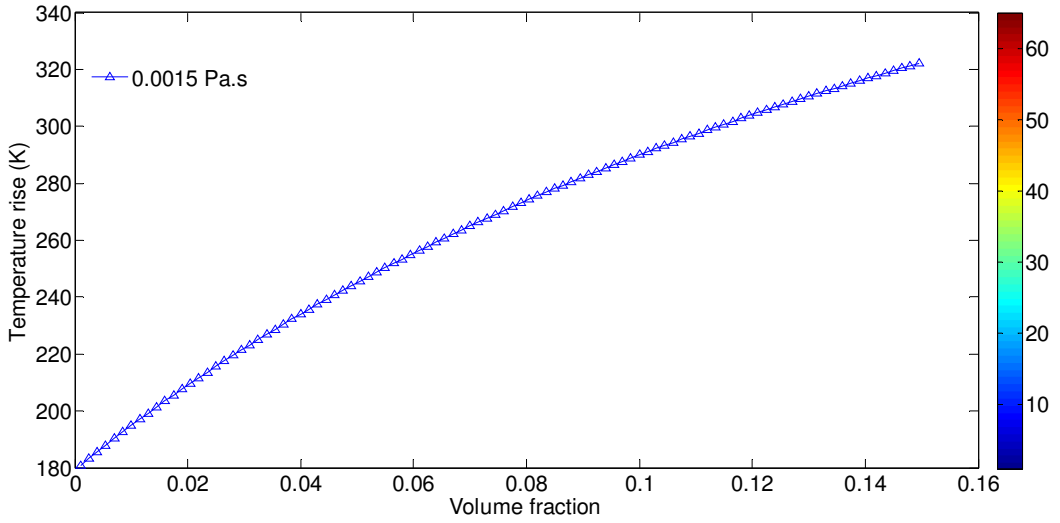

Fig 4.5: Temperature rise as a function of increasing volume fraction of nanoparticles at a fixed viscosity

The heat dissipated by the nanoparticles is computed as the volumetric heat dissipation and as such, increasing their volume fraction will result in increased temperature rise. It is observed that the therapeutic temperature is obtained for volume fractions between 0.12 and 0.14.

4.2 SIMULATIONS

Based on the modeled geometry of the implant and its environment, ABAQUS/CAE 6.9 was used to simulate the temperature profile of the model. The appropriate boundary conditions were imposed on the geometry considering the computational results from the heating of the nanoparticles. In the preliminary simulation, the thermal properties of water were used followed by that of the tumor as given by Ekstrand et al [40]. Below is the table of parameters of the tumor for simulation.

Table 4.1: Parameters of thermal conductivity of tumor used in simulation [40]

Property	Specific Heat ($kJkg^{-1}{}^{o}C^{-1}$)	Thermal Conductivity ($Wm^{-1}{}^{o}C^{-1}$)	Density (kgm^{-3})
Tumor	3.5	0.28	1000

4.2.1 2D TEMPERATURE SIMULATION

In the 2D simulation, the boundary of the tumor was fixed at the temperature of the human body being 37^{o}C and that of the implant and tumor fixed to different values of 55^{o}C, 52^{o}C and 45^{o}C. These are considered the maximum temperature due to the heat generated by the nanoparticles and PDMS gel matrix. The heating step in the Abaqus procedure was referred to as the heating period of the matrix to reach the maximum temperatures mentioned above. The temperature step then represented the temperature gradient created between the boundary of the implant and the tumor outer boundary resulting in the heat conduction.

The 2D planner modeling space, deformable type and shell basic features were used for the geometry of the implant and its environment. The maximum time for the time integration was set at 10000s approximately 2.7 hours. Below are graphs of the temperature simulations for a maximum temperature of 55^{o}C.

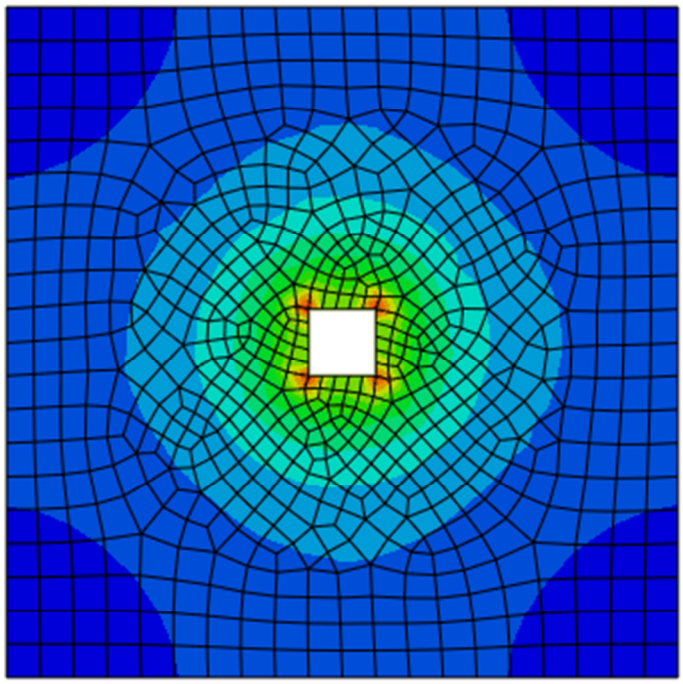

Fig 4.6: Simulation of Heat flux at integration points with exterior edges of the mesh

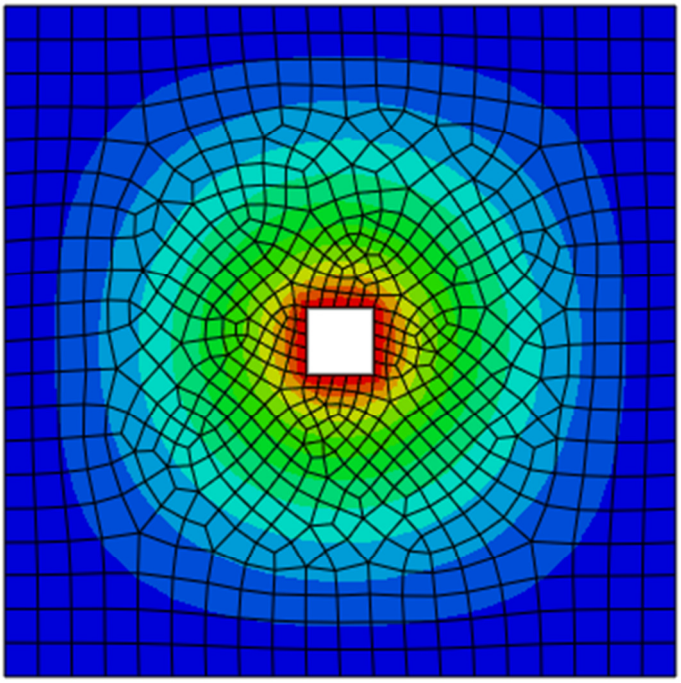

Fig 4.7: Simulation of nodal temperature at nodes with exterior edges of the mesh

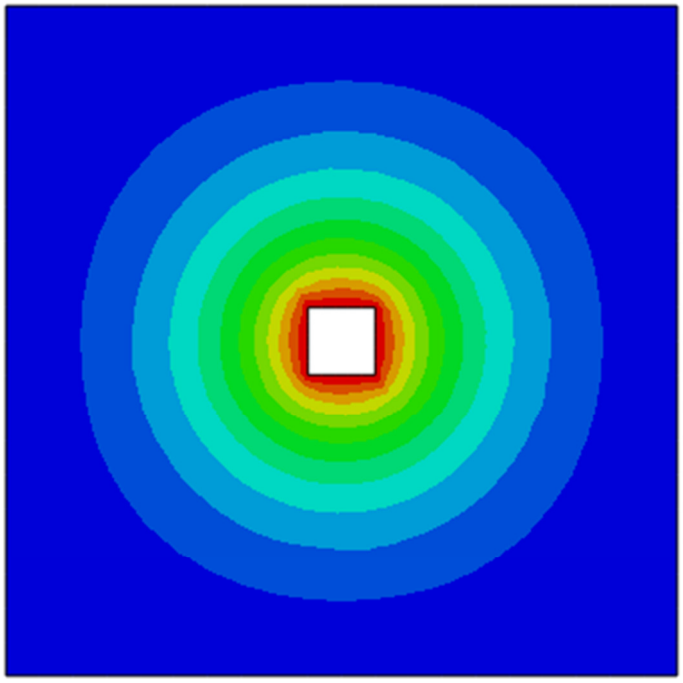

Fig 4.8: Simulation of nodal temperature at nodes with free edges of the mesh

According to Pankhurst et al [18], the temperature of the tumor must be maintained at 42°C and above for at least thirty minute (30min) or more to achieve tumor destruction. It is therefore important to examine the temperature of various nodes relative to the position of the implant.

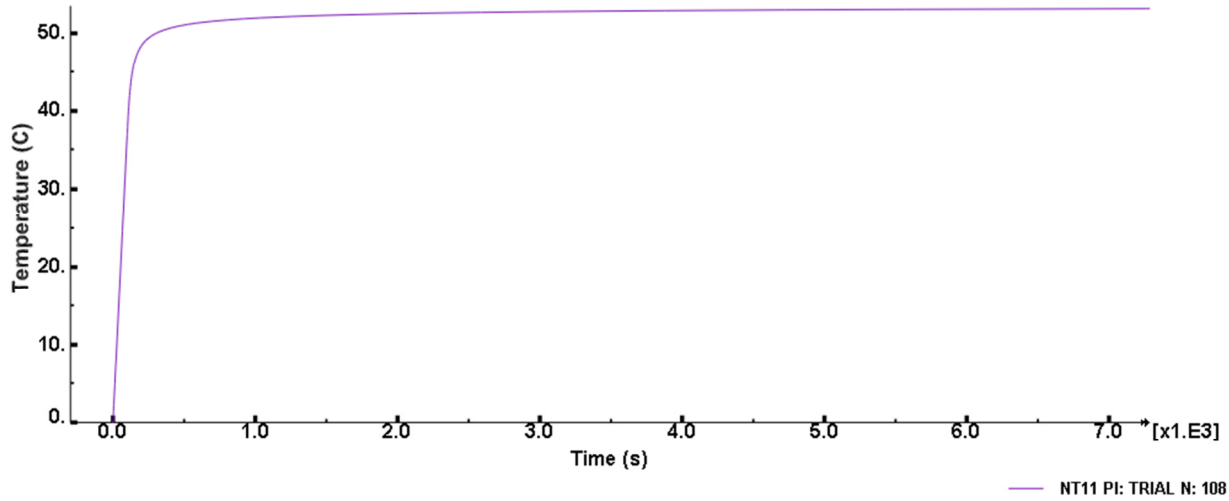

Fig 4.9: Temperature profile of Nodal point very close to the boundary of the implant

The temperature of the nodal point (N:108) very close to the boundary of the implant rise up steady to about 52°C and saturates after 1000s. This temperature difference between the boundary of the implant and of the node is due to size of the element node and to the fact that there is heat flux from the boundary to other parts with time. Hence, the temperature of the tumor around the implant will remain within the therapeutic range.

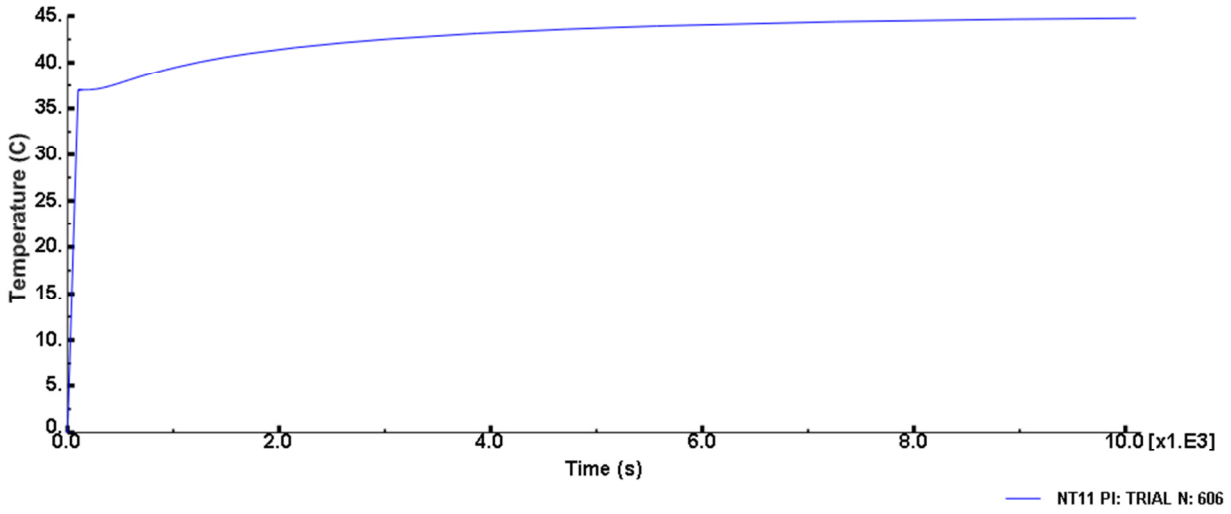

Fig 4.10: Temperature profile of nodal point in the middle of the tumor

In the middle of the tumor, the nodes will obtain the temperature of the human body and then begin to rise until it saturates at about 43°C. This temperature is maintained for the rest of the time for the therapy.

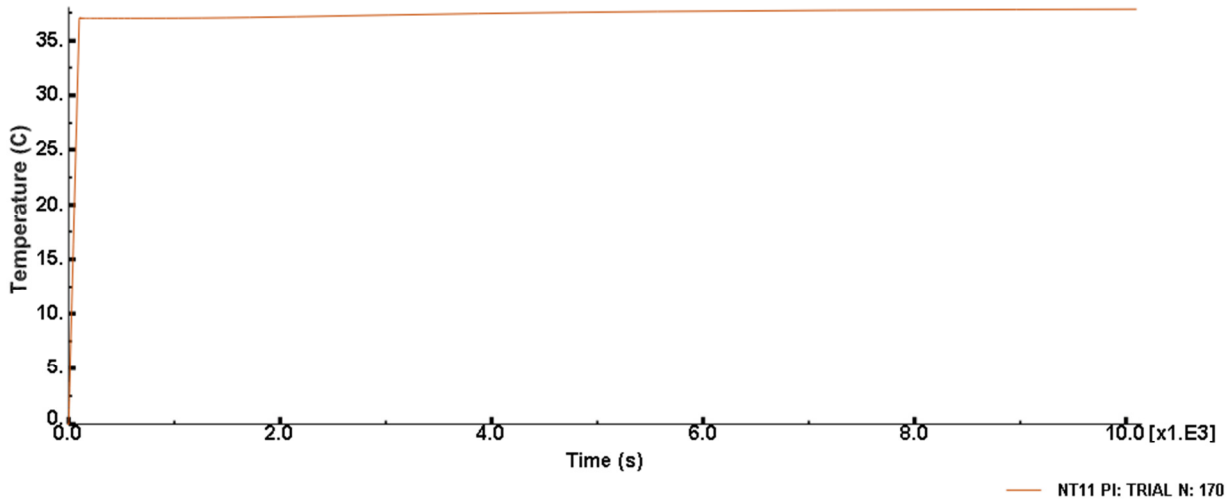

Fig 4.11: Temperature profile of nodal point close to the boundary of the tumor

The nodal points at the boundary of the tumor maintain the body temperature which is found to be appropriate since it would not affect the temperature of healthy tissue around the tumor during therapy. Below is a combined plot showing the temperature profile of the various nodal points in the geometry of the model.

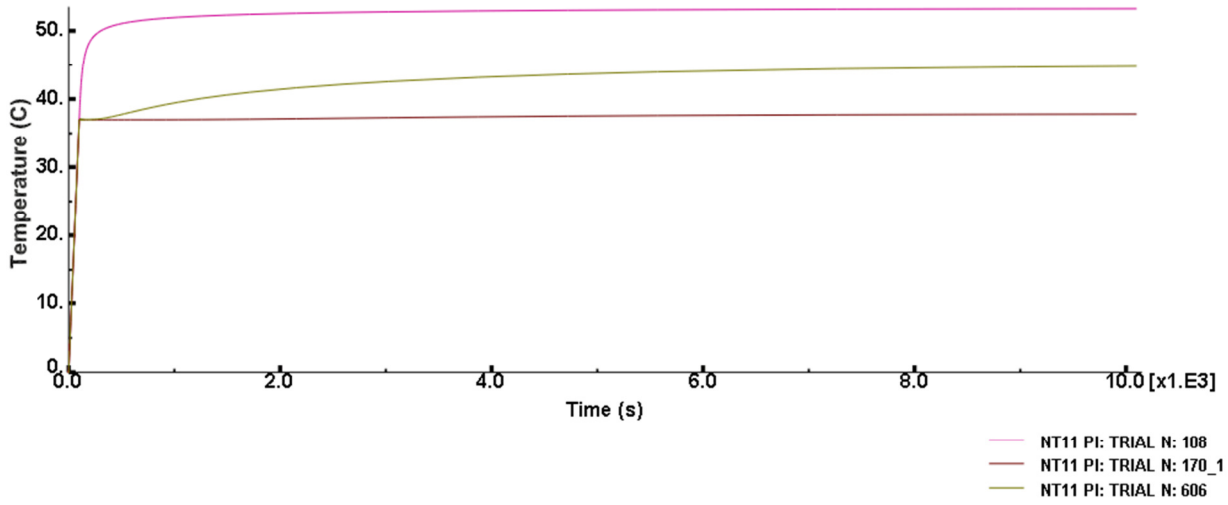

Fig 4.12: Plots of nodal points relative to the boundary of the implant and tumor

Clearly, node N:108 represent nodal points very close to the implant whose temperature rise from the body temperature to saturation whereas N:606 represent those very close to the boundary of the tumor apparently exhibiting body temperature. However, in the middle of the tumor, N:170_1 shows that the temperature of such nodes will rise rapidly above the body temperature to a therapeutic value of about 43^{o}C.

The maximum temperature of the heat generated was reduced to 52^{o}C in the simulation to observe the temperature profile of the tumor.

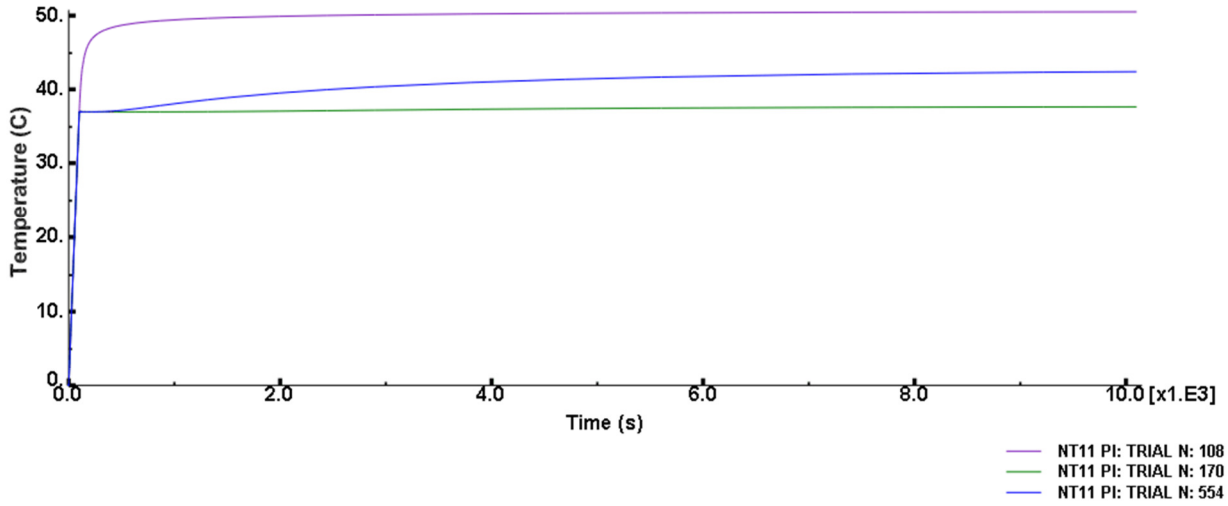

Fig 4.13: Plots of nodal points relative to the boundary of the implant and tumor (52oC max)

The temperature trends of the nodal point's remains the same but for the maximum temperature of the points close to the implant and that in the middle of the tumor that are seen to be occurring approximately at 49^{o}C and 41^{o}C respectively. This model is also found appropriate for hyperthermia.

A lower value of 45^{o}C was also used as the maximum generated temperature in the simulation.

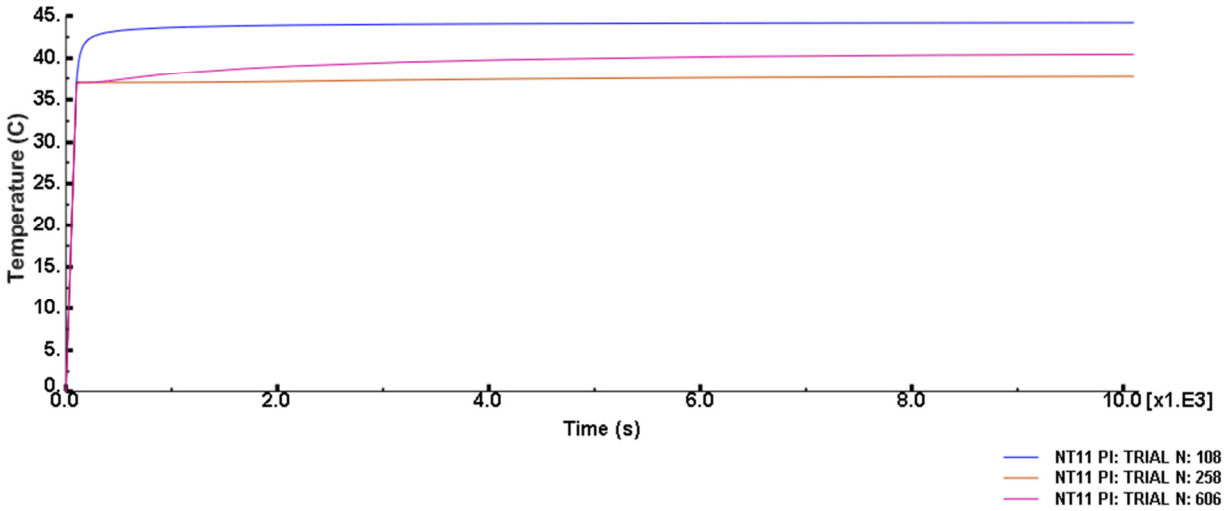

Fig 4.14: Plots of nodal points relative to the boundary of the implant and tumor (45oC max)

Similarly, the temperature trends remain the same. The temperature value of nodes around the implant saturates around 43^{o}C while that within the tumor was 39^{o}C. This is rather lower than the therapeutic value of 42^{o}C but for longer time scales, this is useful in the treatment of the tumor.

4.2.2 3D TEMPERATURE SIMULATION

The deformable solid shape in the 3D modeling space with extrusion was used to create the geometry for the simulation. Also, the necessary boundary conditions together with the appropriate steps for heating and heat conduction were imposed. A graph of the simulation is shown below.

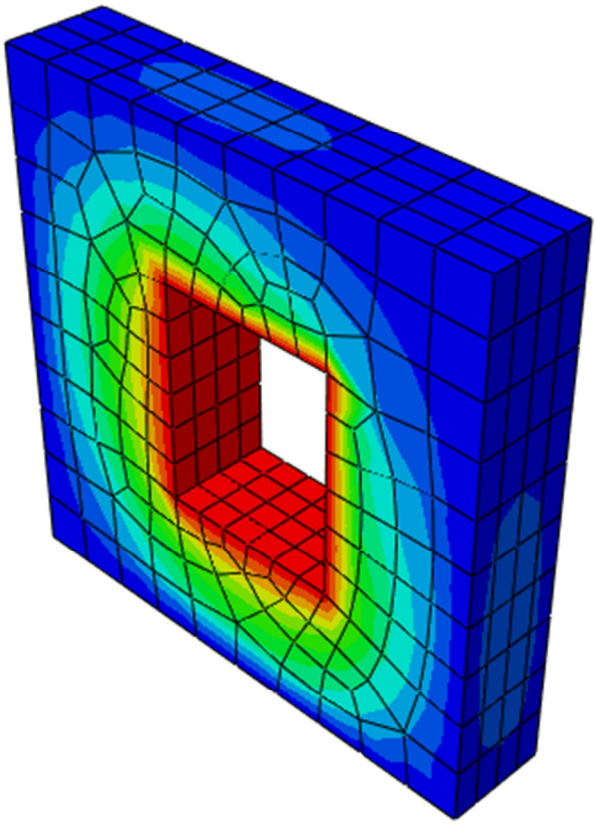

Fig 4.15: Simulation of nodal temperature at nodes with exterior edges of the mesh

The temperature profile of the nodes showed similar trends as in the 2D simulation even though fewer nodes exist in this geometry due to limited number of nodes in this package.

CHAPTER FIVE

CONCLUSIONS AND FUTURE WORK

5.1 CONCLUSIONS

A mathematical model of the implantable biomedical device for localized hyperthermia and drug delivery was developed. A numerical solution of the model was also solved using MATLAB. The geometry of the device and its surrounding tumor was also modeled and incorporated into ABAQUA/CAE software package for Finite Element Simulation. The following can therefore be deduced;

- The temperature rise of the nanoparticles-PDMS matrix is strongly dependent on the frequency and amplitude of applied field, volume fraction of the nanoparticle and viscosity of the PDMS gel.
- The therapeutic temperature of $41^{o}C$ – $46^{o}C$ can be achieved with the following range of parameters;
    - Frequency 2.16 – 2.19 kHz
    - Field amplitude 9.77 – 9.87 kA/m
    - Viscosity 1.1 – 1.2 mPa.s
    - Volume fraction 0.12 – 0.14
- Simulation of the heat diffusion profile shows that the temperature within the tumor can be maintained within the therapeutic range for maximum generated heat of $55^{o}C$ and $52^{o}C$. This is observed not to affect the surrounding healthy tissues since the temperature at the boundary of the tumor is not affected.
- Temperature of the tumor for maximum generated temperature of $45^{o}C$ is seen to fall below the therapeutic value but at longer time scales will be useful in treatment of the tumor.
- For a drug loaded temperature sensitive hydrogel in the device, the heat generated by nanoparticles is enough serve as the transition temperature for the drug release since drug release kinetics of the PNIPA gel generally occurs between $37^{o}C$ and $45^{o}C$.

5.2 FUTURE WORK

The professional version of ABAQUS/CAE can be used to repeat the simulations to have a clear picture of the temperature distribution since the student version is only limited to one thousand nodes (1000) making the element size quite bigger in the 3D simulation.

Swelling of the drug loaded temperature sensitive hydrogel should be included in the modeling and simulation as well as the diffusion kinetics of the drug.

Resistive heating of the device will also be considered in the modeling so as to compare the results with that of inductive heating with magnetite nanoparticles in the PDMS.

REFERENCES

[1] Young-Eun Choi, Ju-Won Kwak and Joon won Park, "Nanotechnology for Early Cancer Detection" Senors 2010, 10, 428-455; doi:10.3390/s100100428

[2] American Cancer Society, Cancer Facts and Figures 2010 Atlanta: American Cancer Society; 2010 pp 2-4

[3] Oyku Akkaya "An Implantable Biomedical Device for Localized Hyperthermia and Drug Delivery" Department of Mechanical and Aerospace Engineering, Princeton University, April 28 2011

[4] Nicholas A. Peppas "Smart Drug Delivery and Bionanotechnology" Center for Biomaterials, Drug Delivery, Bionanotechnology and Molecular Recognition, Department of Chemical and Biomedical Engineeing, The University of Texas at Austin, 1 University Station, Code C0400, Austin, TX7812, USA

[5] S. Zafar Razzacki, Prasanna K. Thwar, Ming Yang, Victor M. Ugaz, Mark A. Burns "Integrated Microsytems for Controlled Drug Delivery" Advanced Drug Delivery Reviews 56 (2004) 185-198

[6] K. Babinch, R. Wyrwa, K. Wagner, T. Seeman, S. Hoeppener, C. Remzi Becer, R. Linke, M. Gottschaldt, J. Weisser, M. Schnabelranch, and U. S. Schubert "Functionalized, Biocompatible Coating for Superparamagnetic Nanoparticles by Controlled Polymerization of a Thioglycosidic Monomer" Biomacromolecules 2011, 12,681-691

[7] Rüdiger Klingeler, Silke Hampel, and Bernd Büchner "Carbon Nanotube Based Biomedical Agents for Heating, Temperature Sensoring and Drug Delivery" Leibniz Institute for Solid State and Materials Research (IFW) Dresden, Helmholtzstr. 20, D-01069 Dresden, Germany

[8] T. Wang, D. Wu, X. Jiang, X. Zhang, Z. Li, J. Zhang, Z. Zheng, R. Zhuo, H. Jiang, and C. Huang "Novel Thermosensitive Hydrogel Injection Inhibits Post Infarct Ventricle Remodeling" European Journal of Heart Failure (2009) 11, 14-19

[9] Cancer Trends Progress Report-2010/2011 updates, National Cancer Institute, NH, DHHS, Bethesda, MD, April 2010, http://progressreport.cancer.gov

[10] www.cancertreatment.pro

[11] Yusuf Olanrewaju Oni, "An Implantable Biomedical Device and Nanoparticles for Cancer Drug Release and Hyperthermia" Department of Mechanical and Aerospace Engineering, Princeton University, September, 2010 pp 8

[12] Bagaria H. G., J. L. Phillips, D. E. Nikles, and D. T. Johnson, "Self-Regulated Magnetic Fluid Hyperthermia", AIChE Annual Meeting Conference Proceedings, 14336-14340, Cincinnati, OH, USA, Oct. 3, 2005.

[13] Gigel Nedelcu "Magnetic Nanoparticles Impact on Tumoral Cells in the Treatment by Magnetic Fluid Hyperthermia" Digest Journal of Nanomaterials and Biostructures vol. 3, No.3, September 2008, p. 103-107

[14] Phillips J. L., "A Topical Review of Magnetic Fluid Hyperthermia", JOSHUA, Vol.3 2005

[15] Pedro Tartaj, María del Puerto Morales, Sabino Veintemillas-Verdaguer, Teresita González-Carreño and Carlos J. Serna, "The Preparation of Magnetic Nanoparticles for Application in Biomedicine" J. Phys. D: Appl. Phys. 36(2003) R182-R197

[16] J. Motoyama, T. Hakata, R. Kato, N. Yamashita, T. Morino, T. kobayashi and H. Honda "Size Dependent Heat Generation of Magnetite Nanoparticles under AC Magnetic Field for Cancer Therapy" BioMagnetic Research and Technology 2008, 6:4 doi:10.1186/1477-044X-6-4

[17] Catherine C. Berry and Adam S. G. Curtis, Topical Review "Functionalization of Magnetic Nanoparticles for Application in Biomedicine" J. Phys. D: Appl. Phys. 36 (2003) R198-R206

[18] Q. A. Pankhurst, J. Connolly, S. K. Jones and J. Dobson, "Application of Magnetic Nanoparticles in Biomedicine", Tropical Review, Journal of Physics D: Applied Physics, 36 (2003) R167-R181

[19] Kamalkumar N. Chauhan, "Finite Element Analysis of Bio-Heat Transfer for Magnetic Fluid Hyperthermia Application", University of Texas, Arlington, December 2009

[20] Williams D. F. "Definition of Biomaterials – Proceedings of a Consensus Conference of the European Society for Biomaterials", 1987 Elsevier, New York

[21] B. Ziaie, A. Baldi, M. Lei, Y. Gu and R. A. Siegel, "Hard and Soft Micromachining for BioMEMS: Review of Techniques and Examples of Application in Microfluidics and Drug Delivery", Advanced Drug Delivery Reviews 56 (2004) 145-172, Elsevier

[22] Rebecca S. Shawgo, Amy C. Richards Grayson, Yawen Li and Micheal J. Cima, "BioMEMS for Drug Delivery", Current Opinion in Solid State and Material Science 6 (2002) 329-334, Elsevier

[23] G. F. Goya, V. Grazu and Ibarra, "Magnetic Nanoparticles for Cancer Therapy", Current Nanoscience, 2008, 4, 1-16

[24] Richard P. Feynman, Robert B. Leighton and Mathew Sands "The Feynman Lectures on Physics, Mainly Electromagnetism and Matter" Oxnard Public Library, 215 South A Street Oxnard, California 93030

[25] David J. Griffiths "Introduction to Electrodynamics" Prentice Hall, Upper Saddle River, New Jersey 07458 pp59

[26] Neil W. Ashcroft and N. David Mermin "Solid State Physics" Saunders College Publishing, Harcourt College Publishers pp 664

[27] Bo Thide "Electromagnetic Field Theory" Upsilon Books, Uppsala, Sweden pp56

[28] Jackson J. D., "Classical Electrodynamics", 3rd Edition, Wiley, 1999, pp 175,6

[29] Richard Fitzpatrick, "Classical Electromagnetism: An Intermediate Level Course", The University of Texas, Austin

[30] Google page www.gitam.edu/eresource/Engg_Phys/semeter_2/magnetic/type.htm

[31] M. R. Ibarra, R. Fernandez-Pacheco, C. Marquina and J. G Valdivia "Biomedical Applications of Magnetic Nanoparticle I: Drug Delivery", Nanotoday 2 (2007) review paper

[32] Li Ying Zhang, Hong-Chen Gu, Xu-Man Wang "Magnetite ferrofluid with High Specific Absorption Rate for Application in Hyperthermia" Journal of Magnetism and Magnetic Materials 311(2007) 228-233

[33] Gilchrist R. K. Medal, R. Shorey W. D., Hanselman, R. C, Parrott, J. C. and Taylor, C. B. (1957) "Selective Inductive Heating of Lymph Nodes", Annals of surgery. 146(4). 596-606

[34] George W. Hanson and S. K. Patch "Optimum Electromagnetic Heating of Nanoparticle Thermal Contrast Agents at RF Frequencies" Journal of Applied Physics 106, 054309 (2009)

[35] Andrzej Skumiel and Mikolaj Labowski, "The Heating Effects of Biocompatible Ferrofluids in an Alternating Magnetic Field" Molecular and Quantum Acoustics vol. 27, (2006)

[36] R. E. Rosensweig "Heating Magnetic Fluid with Alternating Magnetic Field", Journal of Magnetism and Magnetic Materials 252 (2002) 370-374

[37] Elisabetta Sieni, "Biomedical Applications of Electromagnetic Fields: Human Exposure, Hyperthermia and Cellular Simulation", CICLO XXIII, Universita' Di Padova, Facolta' Di ingegneria

[38] A. Thom and C. J. Apelt, "Field Computation in Engineering and Physics", London: D. Van Nostrand 1961

[39] Atkinson W. J., Brezovich I. A. and Chakraborty D. P., "Usable Frequencies in hyperthermia with thermal seeds" 1984, IEEE Trans. Biomed. Eng. BME 31 70-5

[40] Vilhelm Ekstrand, Hans Wiksell, Inkeri Schultz, Bengt Sandstedt, Samuel Rotstein and Anders Eriksson, "Influence of Electrical and Thermal Properties on RF ablation of Breat Cancer: is the Tumor Preferentially Heated?", Biomedical Engineering Online, July 2005, 4:41

APPENDICES

```
% MATLAB code for computing the temperature rise of PDMS Nanoparticle
% matrix
clear all
close all
t = 240;                              %exposure time
C = 1.6518e6;            %specific heat of matrix at fixed volume fraction
Kb = 1.38*10^-23;                     %Boltzman constant
T = 310;                              %Body temperature of the tissue
%eta = 0.001;                         %viscosity in Pa.s ie 1000cs
Md = 446*10^3;                        %Domain magnetization
Vm = 1.4368e-24;
mu = 4*pi*10^-7;                            %permeability of free space
teff = 1.1003e-6;                           %effective relaxation time
Phi = 0.071;                                %volume fraction of nanoparticles
Chi = 1.9868;                               %initial susceptibility
Ho = [5000:70:11930];                       %amplitude of field
f = [8000:200:27800];                       %frequency
 DeltaT = zeros(100,100);                   %Temperature rise matrix
for i = 1:100                               %loop for various field strenghts
    H_1 = Ho(i);
    B = H_1/sqrt(2);                        %field strength
    xi = mu*Md*B*Vm/(Kb*T);                 %Langevin parameter
    Chi0 = Chi*(3/xi)*(coth(xi)-(1/xi));  %Static susceptibility
                                            %DeltaT for different frequencies
    for j = 1:100                           %loop for various frequencies
        w = f(j);
        P = mu*pi*Chi0*H_1^2*w*2*pi*w*teff/(1+(2*pi*w*teff)^2);
        %power dissipation
        DeltaT(i,j) = P*(t/C);                          %Temperature rise
    end
    plot(f(1,[1:100]),DeltaT(i,[1:100]),'-^'); hold all
    %tittle('Temperature rise againts frequency')
    %xlabel('Frequency (Hz)')
    %ylabel('Temperature (K)') %hold all
    %mesh(f,Ho,DeltaT)
end
```

```
%MATLAB code for calculating the temperature rise for varying viscosity and
%volume fraction of the nanoparticles
clear all
close all
D1 = 5180;                                  %density of nanoparticles
D2 = 970;                                   %density of PDMS at 1000cs
Cp1 = 670;                                  %specific heat of nanoparticles
Cp2 = 1350;                                 %specific heat of PDMS
Tn = 2.2631*10^-6;                          %Neel Relaxation time
Vh = 3.0536*10^-24;
t = 240;                                    %exposure time

Kb = 1.38*10^-23;                           %Boltzman constant
T = 310;                                    %Body temperature of the tissue
%eta = 0.001;                               %viscosity in Pa.s ie 1000cs
Md = 446*10^3;                              % Domain magnetization
Vm = 1.4368e-24;
mu = 4*pi*10^-7;                            %permeability of free space
Chi = 1.9868;                               %initial susceptibility
Ho = 9890;                                  %amplitude of field
B = Ho/sqrt(2);                             %field strength
f = 21948;                                  %frequency
xi = mu*Md*B*Vm/(Kb*T);                     %Langevin parameter
Phi = [0.001:0.0015:0.15];                  %volume fraction
Eta = [0.0005:0.00001:0.00149];             %viscosity in Pas
DeltaT = zeros(100,100);
for i = 1:100                             %loop for various volume fraction
    Phi_1 = Phi(i);
    Chi_i = mu*Phi_1*Md^2*Vm/(3*Kb*T);     %initial susceptibility
    Chi0 = Chi*(3/xi)*(coth(xi)-(1/xi));   %Static susceptibility
    Deff = Phi_1*D1+(1-Phi_1)*D2;          %Effective density of the matrix
    Cp = Phi_1*Cp1+(1-Phi_1)*Cp2;          %Effective specific heat
    C = Deff*Cp;
    for j = 1:100                          %loop for various frequencies
        eta = Eta(j);
        Tb = (3*eta*Vh)/(Kb*T);            %Brownian relaxation time
        teff = Tn*Tb/(Tn+Tb);              %Effective relaxation time
        P = mu*pi*Chi0*Ho^2*f*2*pi*f*teff/(1+(2*pi*f*teff)^2);
        DeltaT(i,j) = P*(t/C);                          %Temperature rise
    end
   plot(Phi(1,[1:100]),DeltaT(i,[1:100]),'-^'); %hold all

    %mesh(Eta,Phi,DeltaT)
end
```

```
%MATLAB code for calculating the Temperature rise of the matrix for
%different exposure times
clear all
close all
%t = 100;                          %exposure time
C = 1.6518e6;           %specific heat of matrix at fixed volume fraction
Kb = 1.38*10^-23;                  %Boltzman constant
T = 310;                           %Body temperature of the tissue
%eta = 0.001;                      %viscosity in Pa.s ie 1000cs
Md = 446*10^3;                     %Domain magnetization
Vm = 1.4368e-24;                   %Volume of nanoparticles
mu = 4*pi*10^-7;                   %permeability of free space
teff = 1.1003e-6;                  %effective relaxation time
Phi = 0.071;                       %volume fraction of nanoparticles
Chi = 1.9868;                      %initial susceptibility
to = [120,180,240,300];
for k = 1:4
    t = to(k);
Ho = [9480:10:9980];                        %amplitude of field
f = [20800:28:22200];                       %frequency
 DeltaT = zeros(50,50)
for i = 1:50                                %loop for various field strenghts
    H_1 = Ho(i);
    B = H_1/sqrt(2);                         %field strength
    xi = mu*Md*B*Vm/(Kb*T);                  %Langevin parameter
    Chi0 = Chi*(3/xi)*(coth(xi)-(1/xi));     %Static susceptibility

    for j = 1:50                             %loop for various frequencies
        w = f(j);
        P = mu*pi*Chi0*H_1^2*w*2*pi*w*teff/(1+(2*pi*w*teff)^2);
        %power dissipation
        DeltaT(i,j) = P*(t/C);                              %Temperature rise
    end

end
plot(f(1,[1:50]),DeltaT(i,[1:5  0]),'-^'); hold all
    %;tittle('Temperature rise againts frequency')
    xlabel('Frequency (Hz)')
    ylabel('Temperature (K)') %hold all
end
```